INSTITUT DE FRANCE
Académie des sciences

Comptes Rendus

Géoscience

Sciences de la Planète

António João Teixeira Oliveira, Helena Cristina Brites Martins and Helena Maria Sant'Ovaia Mendes da Silva

Petrogenetic constraints on the felsic vein magmatism in northern Portugal based on petrological and geochemical data

Volume 353, issue 1 (2021), p. 377-398

Published online: 8 December 2021

https://doi.org/10.5802/crgeos.100

Les Comptes Rendus. Géoscience — Sciences de la Planète *sont membres du Centre Mersenne pour l'édition scientifique ouverte*
www.centre-mersenne.org
e-ISSN : 1778-7025

Comptes Rendus
Géoscience — Sciences de la Planète
2021, 353, nº 1, p. 377-398
https://doi.org/10.5802/crgeos.100

Original Article — Petrology, Geochemistry

Petrogenetic constraints on the felsic vein magmatism in northern Portugal based on petrological and geochemical data

António João Teixeira Oliveira *, a, b, **Helena Cristina Brites Martins** a, b and **Helena Maria Sant'Ovaia Mendes da Silva** a, b

[a] Faculdade de Ciências da Universidade do Porto, Departamento de Geociências, Ambiente e Ordenamento do Território, Rua do Campo Alegre, s/n, 4169-007 Porto, Portugal

[b] Instituto de Ciências da Terra, Polo do Porto, Rua do Campo Alegre, s/n, 4169-007 Porto, Portugal

E-mails: up201107754@edu.fc.up.pt (A. J. T. Oliveira), hbrites@fc.up.pt (H. C. B. Martins), hsantov@fc.up.pt (H. M. S. M. da Silva)

Abstract. Three of the largest granite porphyries of northern Portugal were studied to improve current knowledge on the regional felsic vein hypabyssal magmatism. All porphyries exhibit microcrystalline groundmasses of variable granularity (composed of quartz, K-feldspar, and muscovite), quartz, K-feldspar, plagioclase, biotite, and cordierite phenocrysts, antirapakivi and rapakivi feldspars, embayments in quartz, and enrichments in rare metal incompatible elements. The veins were emplaced along fractures generated during the last phase of the Variscan orogeny. Textural features were presumably conditioned by fast cooling, volatile loss, subsolidus annealing, and the magnitude of thermal contrasts at the time of emplacement. All veins were altered by subsolidus hydrothermal fluids, as suggested by several petrographic and geochemical evidence. The generation of mantled feldspars is probably related to isothermal decompression and magma mixing, which is compatible with the εNd_i signatures (−3.76 to −4.40). Based on this research, both processes have contributed to the petrogenesis of the studied porphyries.

Keywords. Granite porphyries, Subvolcanic magmatism, Central Iberian zone, Antirapakivi and rapakivi textures, Microstructures, Whole-rock geochemistry.

Manuscript received 29th July 2021, revised 4th November 2021, accepted 17th November 2021.

1. Introduction

Rock masses and veins that reveal porphyritic texture and a microcrystalline groundmass are generally known as porphyries. Originally, the word "porphyry" was used to describe rocks with a red aphanitic paste, similar to jasper, that enveloped quartz and feldspar phenocrysts [American Geological Institute, 1962]. Nowadays, the term refers to hypabyssal or subvolcanic rocks revealing either felsic or mafic phenocrysts and a fine-grained groundmass. However, at present, porphyry composition

* Corresponding author.

is still a matter of debate. While the majority of the geoscientific community believes that porphyries are mainly felsic [e.g. Vaasjoki et al., 1991, Förster et al., 2007, Wang et al., 2020], some authors argue that their mineral assemblages can be either felsic or mafic [e.g. Damian et al., 2009, Jokela, 2020]. For purposes of clarification, the terminology adopted in this paper always refers to felsic hypabyssal rocks whose mineralogy is granitic or rhyolitic and whose texture is subvolcanic to volcanic.

In both Portugal and Spain, the areas belonging to the Central Iberian Zone are rich in hypabyssal veins of felsic (granitic or rhyolitic porphyries) and mafic (lamprophyres and dolerites) composition. However, even though the existence of these lithologies has been recognized since the 20th century [e.g. Alibert, 1985], extensive studies of subvolcanic rocks in northern Portugal have not begun until recently [e.g. Oliveira et al., 2018, 2019a,b, 2020]. As such, the current state of knowledge about porphyries and mafic dykes in the portuguese section of the Central Iberian Zone (CIZ) is extremely poor. Even though there are several papers concerning the occurrence, petrography, geochemistry, and geochronology of mafic veins in the Spanish CIZ [e.g. Alibert, 1985, Bea et al., 1999, Bonin, 2004, Orejana et al., 2008], detailed studies regarding felsic porphyries in this section of the largest geotectonic/tectonostratigraphic Iberian zone are relatively scarce [e.g. Corretgé and Suárez, 1994]. In their work, Corretgé and Suárez [1994] studied the petrography, microstructures, geochemistry, and mineral chemistry of a garnet and cordierite-bearing granitic porphyry dyke containing rapakivi feldspars in the Cabeza de Araya batholith (Central Spain). These authors suggested that the mineral assemblage of the porphyry resulted from nearly isothermal decompression during fast magma ascent. The rapid kinematics would also be responsible for microstructures such as kinks in biotite and corrosion gulfs in early feldspar crystals, the development of late-stage generations of biotite and cordierite, and the albite and potassium feldspar rims around ovoid, earlier alkali-feldspar crystals.

Two of the most geographically expressive porphyry outcrops in northern Portugal are found in the Vila Pouca de Aguiar and Vila Nova de Foz Côa regions. Besides being regionally significant, these porphyry veins are reasonably well preserved, enabling a proper petrographic and geochemical study.

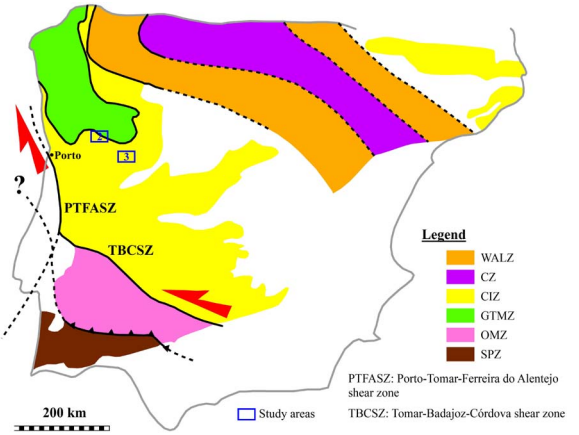

Figure 1. Location of the study areas (2: Vila Pouca de Aguiar; 3: Vila Nova de Foz Côa) in the Iberian Massif setting [adapted from Dias et al., 2016]. Geotectonic zones: WALZ—West Asturian-Leonese Zone; CZ—Cantabrian Zone; CIZ—Central Iberian Zone; GTMZ—Galicia-Trás-os-Montes Zone; OMZ—Ossa-Morena Zone; SPZ—South Portuguese Zone.

This paper reports the petrography, texture, microstructures, whole-rock geochemistry, and Sm–Nd isotope geochemistry of the Vila Pouca de Aguiar (VPA) and Vila Nova de Foz Côa (VNFC) porphyries. The main goal of this research is to improve the state of knowledge concerning the petrogenesis of the felsic vein magmatism in the Central Iberian Zone, with particular emphasis on the portuguese territory.

2. Geological setting

The study areas are located in northern Portugal, in the Iberian Massif, and belong to the Central Iberian Zone (CIZ) (Figure 1). The main geological and geodynamic features of the CIZ were strongly conditioned by the Variscan orogeny. According to Martínez Catalán et al. [2009], the Variscan cycle resulted from the collision between the continental masses of Laurentia and Gondwana. The collisional event happened around 380 Ma (Upper Devonian to Lower Carboniferous) and its effects ceased during Lower Permian times (around 280 Ma).

In NW Portugal, the Variscan orogeny is associated with three main ductile deformation phases (D_1, D_2, and D_3) and one brittle post-tectonic D_4 phase [Dias and Ribeiro, 1995, Martins et al., 2014]. When

the crustal thickening and shortening ceased, the regional tectonics shifted to a regime of subvertical transcurrent shears that characterize phase D_3 [Dias et al., 2010]. The latter generated vertical ductile shear zones in lower structural levels and conjugated brittle fracture systems, with NNE–SSW and NNW–SSE trends, in the upper levels [Marques et al., 2002]. During phase D_3, the regional extension compensated the thickening, causing lithospheric decompression that led to a thermal peak. The decompression triggered anatexis on different crustal levels, which resulted in the generation of several anatectic granite melts displaying a remarkably high compositional variability [Dias et al., 2010, Martins et al., 2009, 2013, Ribeiro et al., 2019]. Since the emplacement of the Variscan granites is mainly related to phase D_3, a classification, based on geochronology, has been proposed to distinguish the granites: syn-D_3 (ca. 320–312 Ma), late-D_3 (ca. 312–305 Ma), late to post-D_3 (ca. 300 Ma), and post-D_3 granites (ca. 299–290 Ma) [Ferreira et al., 1987, Azevedo and Valle Aguado, 2013, Martins et al., 2014, Cruz, 2020].

The Vila Pouca de Aguiar (VPA) region is approximately located 117 km to the northeast of Porto, in northern Portugal. Two porphyries of granitic/rhyolitic composition intrude into the post-tectonic (i.e., post-D_3) VPA pluton, whose main facies are the Vila Pouca de Aguiar and Pedras Salgadas granites. The VPA granite is biotite-rich, medium to coarse-grained, and porphyritic, while the PS (Pedras Salgadas) facies is biotite and muscovite-rich, medium-grained, and porphyritic as well. According to Martins et al. [2009], U–Pb zircon analyses yield an emplacement age of 299 ± 3 Ma. The pluton is a laccolith, and its emplacement was controlled by the sinistral Penacova-Régua-Verín strike-slip fault [Sant'Ovaia et al., 2000]. The porphyries are located on the northeastern section of the pluton and have been named the Loivos vein, at west, and Póvoa de Agrações vein (PA), at east [Oliveira et al., 2019a,b, 2020]. Both structures are N–S trending, about 45 m wide, and ca. 7 km long (Figure 2). Field studies have shown that the western vein only intersects the VPA granite, and always reveals sharp contacts. However, in one location, a microgranite was detected in the contact between the porphyry and host granite. On the other hand, the PA vein intrudes both the Vila Pouca de Aguiar granite and quartzphyllites of the Santa Maria de Émeres Unit [Silurian age; Sant'Ovaia et al., 2011], which belongs to the parautochthonous of the Galicia-Trás-os-Montes Zone (GTMZ). Near the contact between the eastern porphyry and the GTMZ quartzphyllites, there is a very fine-grained, compact, and banded lithology in close association.

Among the various porphyry outcrops in northern Portugal, the vein located in the Vila Nova de Foz Côa (VNFC) region stands out as a special case. The VNFC porphyry is situated about 125 km to the east of Porto, approximately 21.1 km long, 10–20 m wide, and E–W trending (in general) with steep plunges to the north. The vein is hosted in a WSW–ENE ductile shear zone and mainly intrudes into several regional Variscan granites, which are mostly muscovite and biotite-rich, as well as syn-tectonic (syn-D_3) [Ferreira et al., 2020]. However, the porphyry also cuts metasedimentary units of the Schist–Greywacke Complex (Figure 3). According to Silva and Ribeiro [1991], the VNFC vein is cut by multiple strike-slip sinistral faults such as the Vilariça, Portela, and Barril faults (NNE–SSW trending), as well as the Seixo fault (WSW–ENE trending). The porphyry outcrops throughout the entire extent of the eastern block of the Vilariça fault, where its local trend shifts between ENE–WSW and WNW–ESE. On the other hand, in the western block, there are three small, ENE–WSW trending dykes of the granitic vein (10–30 m long), which most likely represent an offset of the porphyry created by the Vilariça fault [Oliveira et al., 2018].

3. Methods

3.1. *Whole-rock geochemistry*

A total of 16 crushed-rock samples (<63 μm) were analyzed for whole-rock geochemical studies. The sample set includes four samples of the Loivos porphyry, four of the PA vein, two samples of the compact lithology that appears in the contact between the Póvoa de Agrações porphyry and GTMZ quartzphyllites, and six samples of the VNFC vein. Sampling site locations are indicated in Figures 2 and 3 (exact coordinates are given in Appendix A). The collected field samples were reasonably fresh and unweathered. Each sample weighed approximately 10 kg.

Whole-rock analyses were performed at the Activation Laboratories in Ancaster (Ontario, Canada). The samples were subjected to lithium metaborate/tetraborate fusion, subsequent Inductively Coupled Plasma and Mass Spectrometry (ICP/MS)

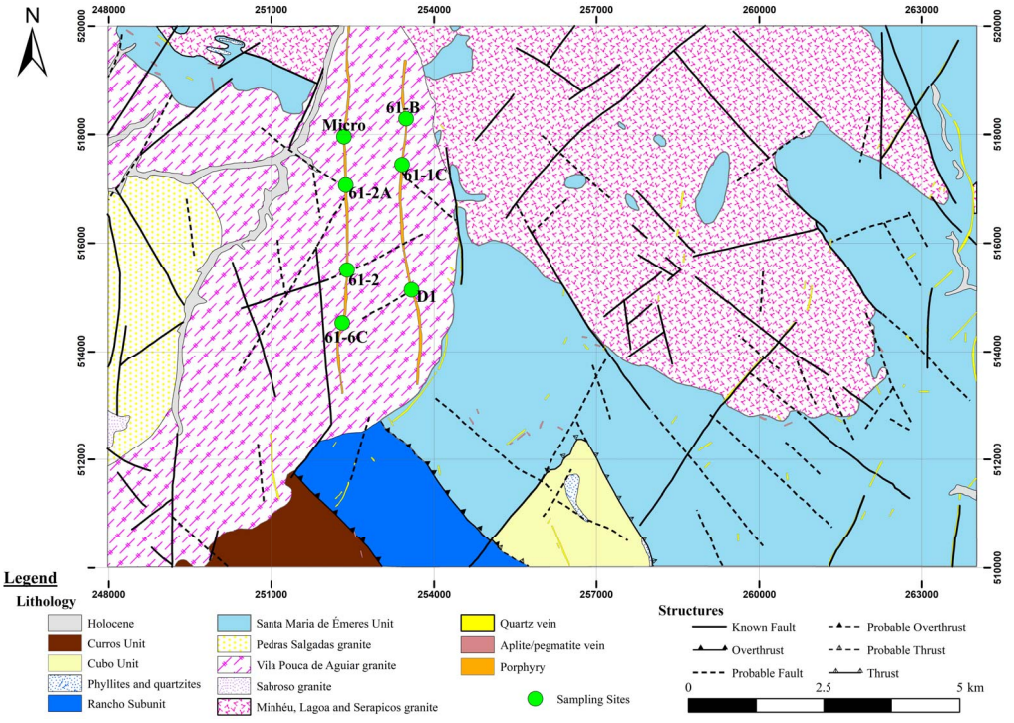

Figure 2. Geological Map of the Vila Pouca de Aguiar region [modified from Noronha et al., 1998]. The Curros, Cubo, and Santa Maria de Émeres Units, as well as the Rancho Subunit, constitute different domains of the GTMZ, all of which are composed of Paleozoic metasediments. All regional granites are Variscan.

analysis, dilution, and reanalysis by a Perkin Elmer Sciex ELAN 6000, 6100, or 9000 ICP/MS equipment. Three blanks and five controls (three before sample group and two after) are analyzed per group of samples. Duplicates are fused and analyzed for every 15 samples. The instrument is recalibrated every 40 samples. For each sample, mass analysis is required as an additional quality control technique, and totals vary between 98.5% and 101%. The detection limits associated with these analyses are the following: 0.01% for major elements; 0.001% for minor elements; and 0.01 to 30 ppm for trace elements.

Sodium peroxide fusion was used to determine lithium contents. Rubidium was also analyzed since the previous technique proved to be inadequate in determining accurate contents of this element in various samples. The procedure requires an initial sodium peroxide fusion followed by acid dissolution. Samples are then analyzed by the Perkin Elmer Sciex ELAN 6000, 6100, or 9000 ICP/MS equipment. A fused blank is run in triplicate for every 22 samples. Fused controls and standards are run after the 22 samples. Fused duplicates are run for every 10 samples. The instrument is recalibrated for every 44 samples. The detection limits of this method, for both lithium and rubidium, are 0.001%.

The studied samples were also fused with a combination of lithium metaborate and lithium tetraborate, in an induction furnace to release fluoride ions from the sample matrix, to determine fluorine contents. Afterward, the fuseate was dissolved in dilute nitric acid, the solution complexed, and the ionic strength adjusted with an ammonium citrate buffer. A fluoride-ion electrode was immersed in the final solution to measure the fluoride-ion activity directly. The detection limit is 0.01%.

3.2. *Sm–Nd isotope geochemistry*

Isotope analyses concerning the Sm–Nd system were executed in Bilbao, Spain, at the Laboratories of General Research Service for Geochronology and Isotopic Geochemistry of the University of the Basque

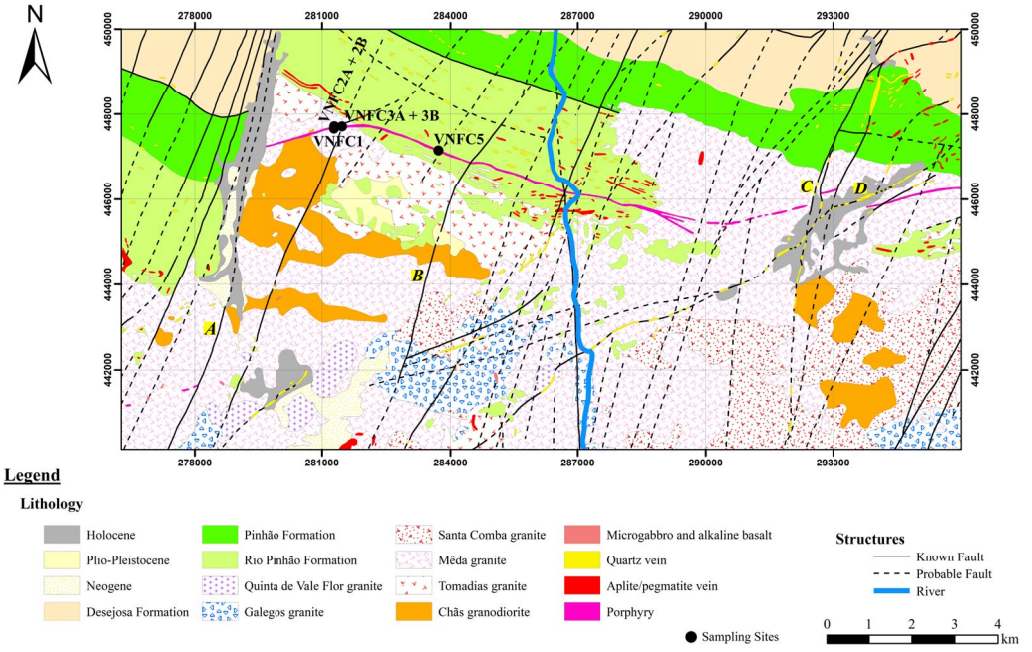

Figure 3. Geological Map of the Vila Nova de Foz Côa region [modified from Silva et al., 1990]. All of the illustrated regional granites are Variscan. The Desejosa, Pinhão, and Rio Pinhão formations represent different metasedimentary units of the Schist–Greywacke Complex. Cenozoic and Quaternary formations are represented by Neogene (conglomerates and arkoses), Plio-Pleistocene (gravel beds), and Holocene (slope deposits, colluvium, and alluvium) cover deposits. The bold italic letters symbolize the most important regional faults: ***A***—Vilariça; ***B***—Portela; ***C***—Barril; ***D***—Seixo.

Country (SGIKER–UPV/EHU). The selected samples were analyzed by ID–MC–ICP-MS (Isotope Dilution–Multi-collector–Inductively Coupled Plasma Mass Spectrometry). About 0.050–0.200 g of each whole-rock sample was weighed and mixed with a proportional amount of an enriched ^{149}Sm–^{150}Nd tracer. The sample-tracer mixtures were digested after a tri-acid attack (HF–HNO_3–$HClO_4$) following the procedures of Pin and Santos Zalduegui [1997]. These procedures were also used for samarium and neodymium purification. For the mass spectrometry, pure Sm and Nd fractions were separately dissolved in 2 mL of 0.32N HNO_3 and diluted to final concentrations of about 30 ng Sm/g and 20 ng Nd/g solutions. The certified reference material JNdi-1 was analyzed to verify the accuracy and reproducibility of the method. The average ^{143}Nd/^{144}Nd ratio of 2 determinations in this standard during the same analytical session was 0.512091, with $2\sigma = 0.000009\sigma$. The precision in the determination of the ^{147}Sm/^{144}Nd ratio by isotope dilution is typically better than 0.2%.

The calculation of the εNd_i parameter was based on the decay constant of Lugmair and Marti [1978] for isotope ^{147}Sm ($\lambda = 6.54 \times 10^{-12}$ y^{-1}), as well as the CHUR ^{143}Nd/^{144}Nd and ^{147}Sm/^{144}Nd ratios of Jacobsen and Wasserburg [1984].

4. Results

4.1. *Petrography and SEM-EDS*

A detailed and thorough petrographic study of the VPA and VNFC porphyries was carried out on a macroscopic and microscopic scale. During the field studies, local magnetic susceptibilities (K_m) were measured using a portable magnetic susceptibility meter, model Terraplus KT-10.

Hand specimen of the Loivos vein exhibit either an indistinguishable grain size or a very fine granularity in the groundmass, which is light gray or light beige (Figure 4a). The granularity of the PA and VNFC porphyries is generally finer and mostly indiscernible to the naked eye, while the groundmasses are

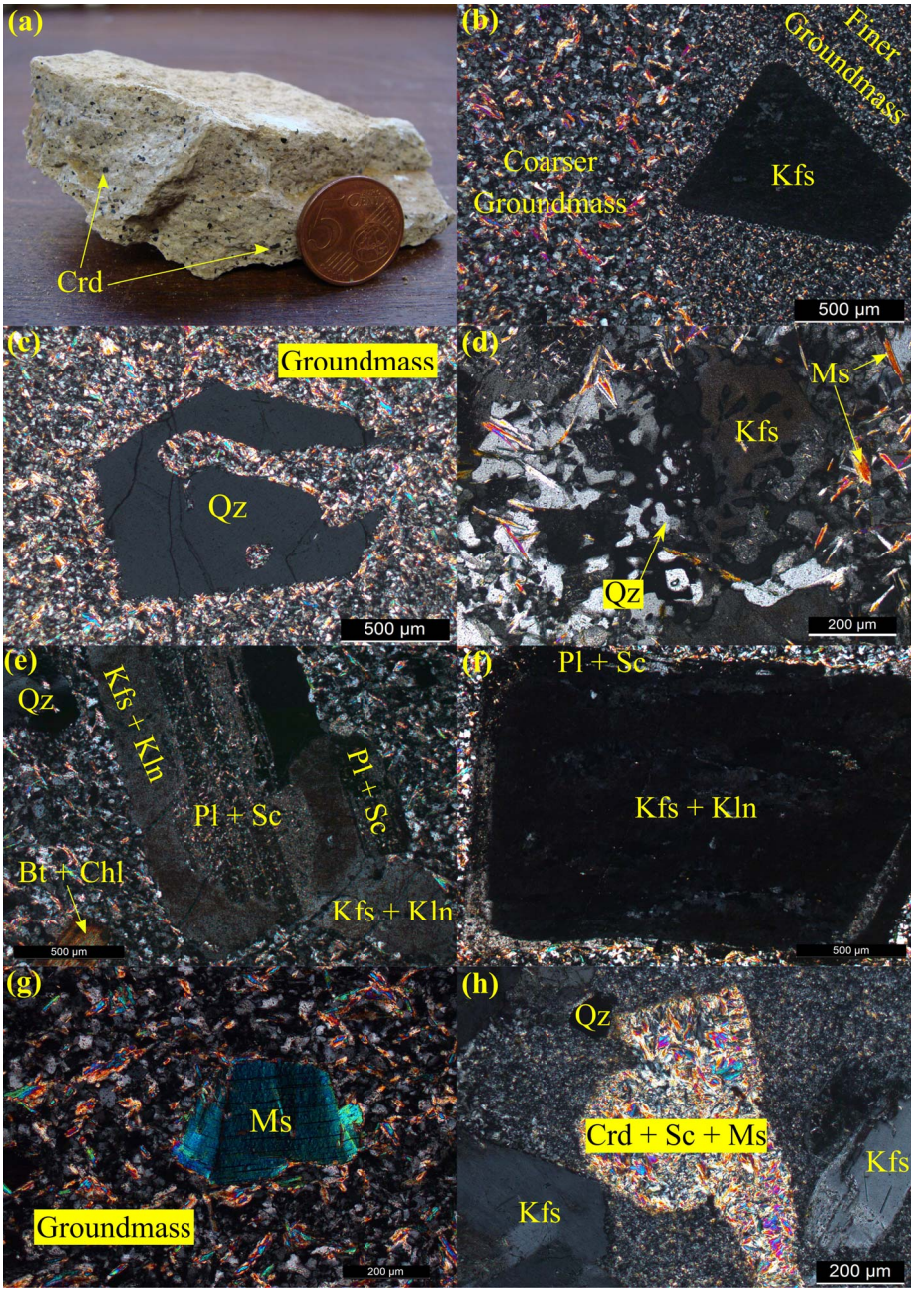

Figure 4. Petrographic photographs and microphotographs of the VPA and VNFC porphyries: (a) hand sample of the Loivos porphyry (sample 61-2); (b) variability of the groundmass granularity (sample 61-1C); (c) embayment on a quartz microphenocryst (sample 61-D); (d) granophyric texture (sample 61-2A); (e) antirapakivi feldspars (sample VNFC2A); (f) rapakivi feldspars (sample 61-1C); (g) kinked primary muscovite microphenocryst (sample 61-1C); (h) pinitization: pseudomorphs of white micas after cordierite (sample 61-2). Legend: Qz—quartz; Kfs—potassium feldspar; Pl—plagioclase; Bt—biotite; Ms—muscovite; Crd—cordierite; Kln—kaolinite; Sc—sericite; Chl—chlorite. All microphotographs were taken in CPL.

respectively greenish or pinkish and light gray to light beige. All samples of the PA vein display a very fine banding and sample VNFC2A of the E–W trending porphyry shows feldspar phenocrysts that seemingly follow the local vein trend (N130° to 145° E). Despite the previous observations, overall, none of the porphyries reveals any sort of anisotropy regarding the orientation of the composing minerals. All veins exhibit abundant phenocrysts, mostly 0.1 to 2.5 cm long, composed of quartz, feldspars, cordierite, and biotite. Several mafic phenocrysts are altered, presenting orange or brownish-colored rims made of Fe oxides. However, in the Loivos porphyry, alteration is more pronounced in the groundmass due to rubefaction. Based on the microscopic studies, all veins display two holocrystalline textures whose differences mostly concern granularity (Figure 4b). In the Loivos porphyry, both textural varieties are aphanitic and porphyritic, while in PA and VNFC, the coarser facies is aphanitic (phenocryst-rich) and the finer facies is aphyric (phenocryst-poor). The groundmasses are mainly composed of quartz, K-feldspar, and muscovite. Apatite, ilmenite, zircon, and monazite are less common but present in all veins. The Loivos and VNFC porphyries also have late-stage chlorite, as well as secondary minerals such as brookite/anatase, hematite, and goethite. Allanite and rare Fe–Mn–Al/Na phosphates (childrenite, scorzalite (?), and gayite (?)) were exclusively observed in the PA vein. Compositionally, the VPA and VNFC porphyries are identical to syenogranites or alkali-feldspar granites. The contacts between the VPA veins and respective spatially associated lithologies (i.e., microgranite for Loivos and compact lithology for PA) are gradual. In both cases, there are strong similarities regarding texture, color, and granularity.

Quartz is the most abundant mineral phase. It occurs either in fine anhedral grains at the groundmass level or in phenocrysts and microphenocrysts. The latter are dominantly anhedral (Loivos porphyry) or subhedral to euhedral (PA and VNFC veins). Grain boundaries are mostly linear or curved. Quartz inclusions in some K-feldspar phenocrysts define lineaments which circumscribe to the shape of the host mineral. In the finer portions of all porphyries, groundmass quartz occasionally reveals a "drop-like" texture. In the PA and VNFC veins, quartz phenocrysts display multiple fractures, which are normally filled either by groundmass grains or Fe oxides. Concerning textures and microstructures, quartz phenocrysts present common embayments (Figure 4c), undulatory extinction, and occasional polygranular aggregates or subgrains. In the boundaries with K-feldspar phenocrysts or microphenocrysts, quartz sometimes reveals granophyric texture (this feature was only observed in Loivos) (Figure 4d).

Potassium feldspar occurs in fine, mostly anhedral groundmass grains, or in phenocrysts and (scarce) microphenocrysts of tabular habit and subhedral to euhedral shape. In all porphyries, Karlsbad twinning is more common than the cross-hatched one. Occasionally, the twinnings are deformed. Perthites are venule, sector, band, or bar type. Together with plagioclase (and sometimes quartz), K-feldspar microphenocrysts form agglomerates in glomeroporphyritic texture, where they also display embayments. While the Loivos porphyry only presents antirapakivi feldspars, the PA and VNFC veins show both antirapakivi and rapakivi. In the antirapakivi crystals, the potassium feldspar rims are incomplete, subhedral, and mostly altered to kaolinite (Figure 4e). In the rapakivi feldspars, the plagioclase rims are either complete or incomplete, mainly euhedral, and usually present myrmekite intergrowths (Figure 4f). K-feldspar in the VPA and VNFC porphyries is mainly orthoclase (± sanidine ± adularia) and occasionally microcline.

Plagioclase is exclusive to the phenocryst and microphenocryst population, exhibiting tabular habit and a predominant subhedral shape. Most crystals reveal polysynthetic twinning and some also show simple twinning. In all cases, oscillatory zoning is uncommon and the phenocrysts exhibit occasional fractures, which may be filled by groundmass minerals. Based on the Michel–Lévy method, plagioclase in all porphyries is, possibly, albite–oligoclase: An_2–An_{12} (Loivos), An_0–An_8 (PA), and An_6–An_{18} (VNFC).

Cordierite is more common in the PA vein. Cordierite crystals are exclusively phenocrysts or microphenocrysts. Their habit is typically tabular or rarely prismatic, while the shape is subhedral to euhedral. Regarding textures and microstructures, cordierite microphenocrysts reveal rare embayments. The latter and the homogeneous distribution of cordierite in thin sections attest to a magmatic origin for this mineral [Alasino et al., 2004].

The VPA and VNFC porphyries are richer in muscovite than biotite. The white mica occurs mostly

at the groundmass level, in very fine grains, with an anhedral or subhedral shape and needle-like habit. However, scarce larger primary muscovite crystals (microphenocryst-like) are also present in the VPA veins. These are subhedral in shape, lamellar in habit, and may present cleavage bending or kinks (Figure 4g).

Biotite occurs in microphenocrysts of lamellar or tabular habit and subhedral shape, whose size is typically smaller when compared to the quartz, feldspar, and cordierite counterparts. The abundance of this mineral is the lowest in the PA porphyry. Fresh biotite reveals many pleochroic halos where prismatic crystals of zircon, monazite, and apatite are included. The dark mica is also frequently associated with late-stage chlorite (whose very fine and anhedral grains display radial texture) and opaque minerals. Microstructures, such as cleavage bending and kinks, were occasionally observed in larger lamellar crystals. In the aphyric facies of the PA and VNFC porphyries, biotite is very scarce and mostly altered to chlorite.

Apatite crystals show prismatic, rounded, or needle-like habits, as well as hexagonal–euhedral or anhedral shapes.

Opaque grains are typically very fine, anhedral or euhedral in shape, and prismatic or needle-like in habit. They are either dispersed throughout the groundmass or included in biotite and cordierite microphenocrysts. All veins have fractures cutting through the groundmass and phenocrysts, which are filled with Fe oxides and/or opaque minerals. Considering the magnetic susceptibility values registered on the field (K_m = 22.03–49.55 μSI [Loivos]; ≈60–81 μSI [PA]; 62.32–74.25 μSI [VNFC]), these opaque crystals are mostly paramagnetic minerals such as ilmenite, which was verified in SEM-EDS. The analysis revealed a Fe–Ti oxide composition, with minor Nb and Ta contents. According to Stimac and Hickmott [1994], both niobium and tantalum are common, albeit minimal, impurities in ilmenite. Vestigial amounts of other oxides, namely columbite–tantalite [$(Mn,Fe)(Ta,Nb)_2O_6$] and cassiterite [SnO_2], have only been detected in PA.

Zircon and monazite are exceptionally rare accessory minerals. Both are mainly included in biotite microphenocrysts, where they are surrounded by pleochroic halos.

Allanite is an extremely rare phase in the mineral assemblage of the PA porphyry. This mineral occurs in prismatic, euhedral crystals, which are closely associated with the biotite or potassium feldspar and occasionally reveal zoning.

Childrenite [$FeAl(PO_4)(OH)_2 \cdot H_2O$], probable scorzalite [$FeAl_2(PO_4)_2(OH)_2$], and gayite [$NaMnFe_5(PO_4)_4(OH)_6 \cdot 2H_2O$] are the least common minerals of the PA vein. These phosphates were identified during the SEM-EDS analysis. Childrenite is the most common, occurring in large phenocryst or microphenocryst-like grains of tabular habit and subhedral or anhedral shape. Childrenite is always associated with feldspar phenocrysts and microphenocrysts. On the other hand, scorzalite and gayite occur in smaller crystals (maximum 100 μm long) of anhedral habit. They are always included in the potassium feldspar phenocrysts. Further analyses are required to confirm the presence of these two minerals.

All porphyries were subjected to post-magmatic alterations as evidenced by the following petrographic features: (i) partial or complete kaolinization of K-feldspar, which sometimes masks the twinnings and perthites; (ii) sericitization and saussuritization of plagioclase; (iii) biotite muscovitization and chloritization; and (iv) cordierite pinitization (all cordierite is completely altered to pseudomorphs of chlorite and white mica (Figure 4h)). Secondary minerals, such as brookite, anatase, and the Fe oxides, resulted from the alteration of biotite and cordierite. The presence of brookite and anatase was confirmed throughout the SEM-EDS analysis after detecting a Ti-oxide composition and minor Nb impurities, which are typical of both brookite and anatase [Werner and Cook, 2001, Barnard et al., 2019]. The respective grains show prismatic habit and anhedral or euhedral shape. On the other hand, the Fe oxides (hematite and goethite mostly) are always anhedral.

4.2. *Whole-rock geochemistry*

The bulk-rock compositions of the VPA and VNFC porphyries are presented in Table 1. As mentioned above, the compact lithology that appears next to the PA vein was also analyzed. For comparative purposes, the geochemical data concerning the respective regional granites [Martins et al., 2009, Ferreira et al., 2020] is illustrated but not described in this paper.

Table 1. Major, minor, and trace element contents of the Vila Pouca de Aguiar and Vila Nova de Foz Côa porphyries

Samples	61-1	61-B	61-1C	D1	61-2	61-2A	61-6Ca	61-6Cb	CC green	CC pink	VNFC1	VNFC2A	VNFC2B*	VNFC3A	VNFC3B*	VNFC5
Lithology	Póvoa de Agrações porphyry				Loivos porphyry				Compact lithology		Vila Nova de Foz Côa porphyry					
SiO_2	72.78	72.42	72.29	72.56	73.19	72.83	74.15	73.07	71.54	71.35	72.32	72.75	73.15	75.37	76.43	73.73
TiO_2	0.055	0.052	0.041	0.042	0.097	0.099	0.102	0.102	0.034	0.032	0.142	0.144	0.068	0.140	0.056	0.152
Al_2O_3	15.77	14.98	15.06	15.83	15.01	14.47	14.35	14.04	16.21	15.72	14.26	14.47	13.95	14.17	13.53	14.60
$Fe_2O_3^t$	0.98	0.90	0.87	0.70	1.03	1.01	1.10	1.10	1.03	0.70	1.07	1.39	0.91	1.36	1.11	1.53
MnO	0.062	0.051	0.051	0.047	0.032	0.025	0.030	0.028	0.060	0.041	0.022	0.033	0.034	0.039	0.062	0.034
MgO	0.11	0.09	0.11	0.08	0.15	0.16	0.18	0.17	0.19	0.05	0.23	0.28	0.22	0.36	0.25	0.29
CaO	0.58	0.56	0.27	0.78	0.47	0.53	0.54	0.53	0.18	0.75	0.47	0.49	0.43	0.17	0.27	0.55
Na_2O	4.02	3.77	4.64	3.80	3.27	3.13	3.24	3.18	3.73	3.98	2.53	2.68	1.68	0.28	0.07	2.94
K_2O	3.92	3.84	3.79	3.84	4.49	4.68	4.67	4.72	3.89	3.80	4.73	4.80	5.01	6.37	4.10	4.64
P_2O_5	0.63	0.75	0.28	0.76	0.40	0.39	0.44	0.42	0.20	0.82	0.30	0.29	0.37	0.25	0.28	0.27
LOI	1.38	1.56	1.13	1.79	1.39	1.43	1.35	1.35	1.88	1.58	3.18	2.65	2.98	2.28	2.46	1.47
Total	100.30	98.98	98.53	100.20	99.54	98.76	100.20	98.70	98.95	98.83	99.25	99.98	98.80	100.80	98.62	100.20
Be	49	42	20	21	6	7	5	5	20	57	5	7	4	5	14	8
Ba	55	58	47	39	82	109	95	91	31	20	185	190	61	191	25	193
Sr	94	68	48	68	23	25	29	28	16	39	42	43	18	36	5	49
Y	10	9	6	10	13	13	14	12	6	7	15	14	5	9	3	15
Zr	46	41	31	38	42	39	48	40	32	30	73	75	30	70	22	80
Rb	1240	1110	856	1370	349	331	339	345	1460	1290	362	362	509	626	508	314
Nb	45	35	35	53	13	10	18	11	47	39	14	13	19	14	14	13
Sn	182	151	209	214	35	23	29	24	344	240	23	24	61	69	69	20
Cs	238.0	271.0	84.1	118.0	34.0	30.8	29.2	29.9	187.0	99.1	23.8	30.7	32.7	36.6	29.7	25.0
La	6.0	5.8	4.3	4.6	7.8	7.6	7.6	7.9	4.6	3.5	14.3	14.3	3.3	15.3	1.3	13.6
Ce	13.9	13.1	9.6	10.4	16.5	17.1	16.5	17.1	8.1	6.6	30.9	33.2	7.2	32.9	3.5	30.0
Pr	1.62	1.67	1.29	1.22	2.23	2.19	1.92	2.17	1.21	0.99	3.58	3.79	0.87	3.81	0.49	3.57
Nd	6.3	5.5	4.3	4.6	7.7	8.0	7.3	7.6	4.2	3.7	13.4	13.6	3.2	13.4	2.2	13.3
Sm	1.6	1.6	1.3	1.2	2.2	2.3	2.0	2.2	1.1	1.2	2.9	3.3	0.9	2.7	0.6	3.1
Eu	0.09	0.10	0.08	0.06	0.15	0.19	0.16	0.15	0.07	0.06	0.26	0.29	0.07	0.23	0.08	0.27
Gd	1.5	1.5	1.1	1.3	2.3	2.3	2.0	2.1	1.1	1.2	3.2	3.1	0.9	2.2	0.6	2.9
Tb	0.3	0.3	0.2	0.2	0.5	0.5	0.4	0.4	0.2	0.2	0.5	0.5	0.2	0.4	0.1	0.5
Dy	1.5	1.6	1.2	1.4	2.6	2.5	2.3	2.4	1.2	1.3	3.0	3.0	0.9	2.0	0.7	2.9
Ho	0.3	0.3	0.2	0.2	0.4	0.4	0.4	0.4	0.2	0.2	0.5	0.5	0.2	0.3	0.1	0.5
Er	0.8	0.7	0.5	0.6	1.1	1.0	0.9	1.0	0.6	0.6	1.5	1.4	0.4	0.9	0.3	1.3
Tm	0.11	0.10	0.08	0.10	0.16	0.14	0.13	0.14	0.09	0.08	0.22	0.20	0.06	0.14	<0.05	0.19
Yb	0.8	0.7	0.6	0.7	1.0	0.9	0.9	0.9	0.7	0.6	1.4	1.3	0.4	0.9	0.3	1.3
Lu	0.12	0.11	0.09	0.10	0.16	0.15	0.13	0.15	0.11	0.10	0.18	0.20	0.06	0.14	0.04	0.19
Hf	3.0	2.3	2.1	3.0	1.7	1.3	1.9	1.3	2.8	2.4	2.3	2.3	1.5	2.7	0.9	2.5
Ta	28.0	29.1	35.5	34.8	4.4	3.7	4.4	4.1	44.5	43.5	4.1	3.8	9.5	4.3	6.8	3.7
W	13	16	6	10	9	7	8	7	10	11	8	10	12	9	12	7
Pb	13	10	15	8	25	13	20	19	<5	13	31	30	30	125	13	20
Th	3.7	3.4	2.5	2.8	4.6	4.7	4.5	4.6	1.8	1.7	9.1	9.9	2.4	9.3	1.8	8.9
U	21.9	17.8	19.3	21.0	14.6	11.4	16.2	16.2	28.5	21.8	7.4	12.6	7.2	9.6	8.5	11.9
Li	850	1030	80	540	120	70	60	60	190	300	120	150	140	110	80	180
F	2600	3200	300	1700	4500	500	300	300	800	1200	600	600	700	600	300	400
ΣREE	34.94	33.08	24.84	26.68	44.80	45.27	42.64	44.61	23.48	20.33	75.84	78.68	18.66	75.32	10.31	73.62
$(La/Yb)_N$	5.06	5.59	4.83	4.43	5.26	5.69	5.69	5.92	4.43	3.93	6.89	7.42	5.56	11.46	2.92	7.05
$(La/Sm)_N$	2.36	2.28	2.08	2.41	2.23	2.08	2.39	2.26	2.63	1.83	3.10	2.73	2.31	3.56	1.36	2.76
$(Gd/Yb)_N$	1.51	1.73	1.48	1.50	1.86	2.06	1.79	1.88	1.27	1.61	1.84	1.92	1.82	1.97	1.61	1.80
$(Eu/Eu^*)_N$	0.18	0.20	0.20	0.15	0.20	0.25	0.24	0.21	0.19	0.15	0.26	0.28	0.24	0.29	0.41	0.28
$TE_{1,3}$	1.11	1.17	1.17	1.14	1.22	1.21	1.14	1.16	1.09	1.09	1.08	1.12	1.11	1.17	n.d.	1.11

Major and minor elements are expressed in weight percentage (wt%), while the trace elements are in parts per million (ppm). Legend: n.d.—not determined. Samples VNFC2B and 3B represent the aphyric facies of the VNFC porphyry. $TE_{1,3}$ is the degree of the tetrad effect [Irber, 1999].

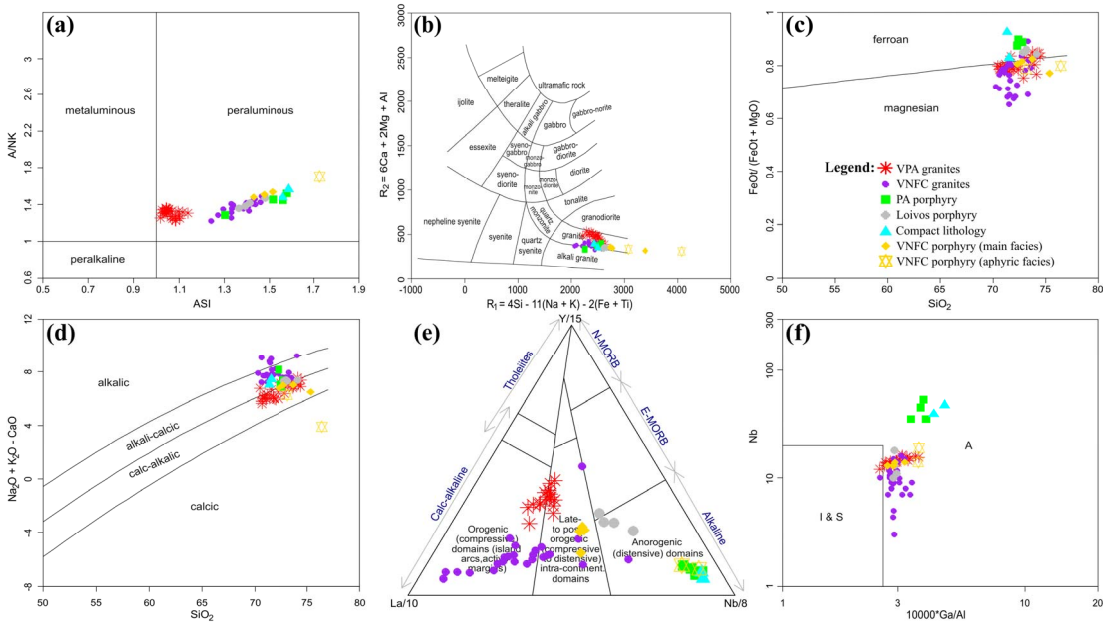

Figure 5. Projection of the VPA and VNFC porphyries in the following diagrams: (a) ASI vs. A/NK [Frost et al., 2001]; (b) R_1 vs. R_2 [De La Roche et al., 1980]; (c) SiO_2 vs. $FeO^t/(FeO^t + MgO)$ [Frost et al., 2001]; (d) SiO_2 vs. $Na_2O + K_2O$—CaO [Frost et al., 2001]; (e) La/10-Y/15-Nb/8 [Cabanis and Lecolle, 1989]; (f) 10,000 × Ga/Al vs. Nb [Whalen et al., 1987].

Based on the results, there is no evidence suggesting the existence of any sort of genetic relationship between the porphyries and granites.

The granitic/rhyolitic porphyries of the VPA and VNFC regions are high-K calc-alkaline rocks and strongly peraluminous, as indicated by their high ASI values (VPA: 1.27–1.45; VNFC: 1.39–1.92) (Figure 5a). In VPA, the compact lithology presents a slightly higher alumina saturation (ASI = 1.42–1.55). On the other hand, the aphyric facies of the VNFC vein displays abnormally high ASI values (ASI = 1.64–2.87), causing the respective samples to be projected outside the normal range of the De La Roche et al. [1980] diagram (Figure 5b). The low Na_2O contents and high ASI suggest that the aphyric rock was significantly affected by post-magmatic alterations. As such, the respective samples cannot be used to gain information about primary magmatic features. For all porphyries, the normative compositions are identical to those of granites (*sensu stricto*) or alkali granites. However, while the VPA veins are ferroan and alkali-calcic, the VNFC specimen is magnesian and calc-alkalic to alkali-calcic (Figures 5c and d). The whole-rock geochemical results suggest that the VPA porphyries are associated with post-orogenic or anorogenic settings, whilst the geochemical signature of the VNFC vein is typical of syncollisional or late to post-orogenic environments (Figure 5e). Also, these subvolcanics lithologies display features resembling those of "A-type" granites [Whalen et al., 1987, Bonin, 2007] (Figure 5f).

When comparing the VPA veins, the Loivos porphyry is richer in SiO_2, $Fe_2O_3^t$, MgO, K_2O, and TiO_2, whereas the PA vein has higher contents in Al_2O_3, Na_2O, and P_2O_5. The compact lithology presents high variability regarding the $Fe_2O_3^t$, MgO, CaO, and P_2O_5 contents. It is also the richest in Al_2O_3 and poorest in TiO_2. On the other hand, the VNFC porphyry presents the highest SiO_2, $Fe_2O_3^t$, MgO, K_2O, and TiO_2 contents, as well as the lowest Al_2O_3, Na_2O, P_2O_5, and CaO contents. When compared to the host pluton, the VPA veins are moderately enriched in P_2O_5 and remarkably enriched in rare incompatible metal elements, namely Li, Be, Rb, Sn, Cs, Nb, Ta, and W. However, both porphyries are depleted in Ba, Sr, Y, Zr, Hf, and Th, and they also present high U and F contents. Despite the small distance between the two veins, the PA porphyry is clearly richer in most of these elements. The compact lithology and PA specimen present an identical trace element composition. The

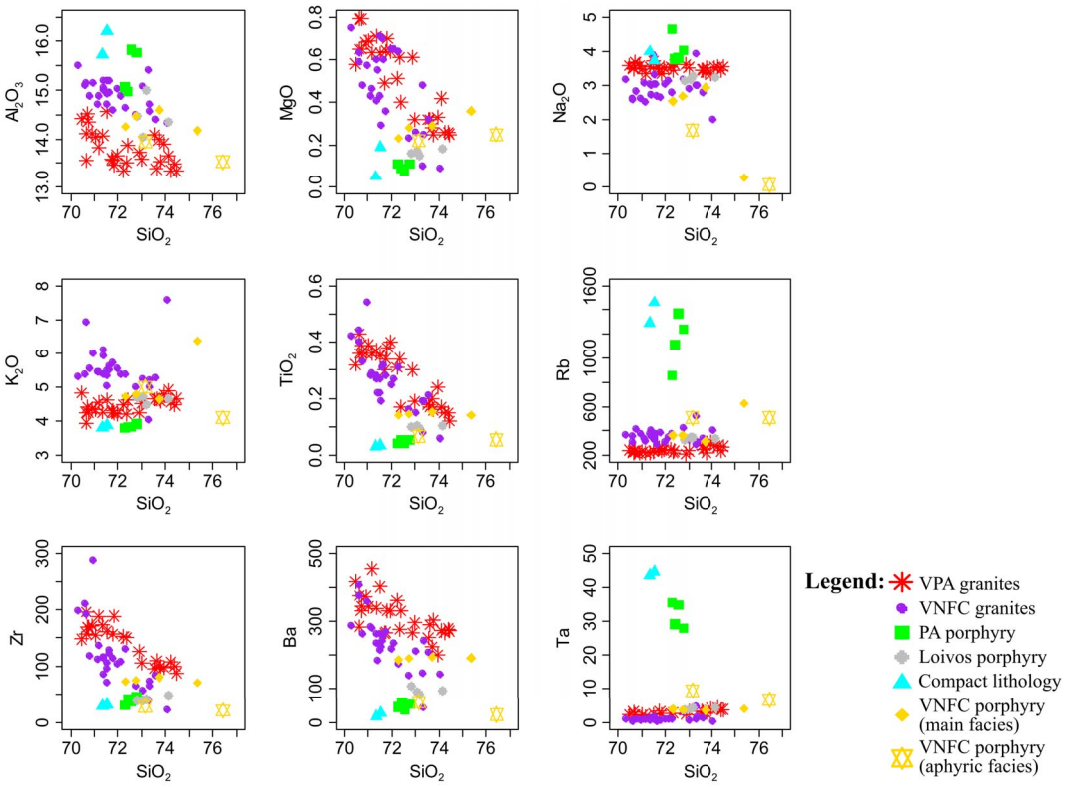

Figure 6. Harker diagrams for major, minor, and trace elements of the VPA and VNFC porphyries.

contents of the aforementioned rare incompatible metal elements in the VNFC vein are similar to those of the Loivos porphyry. However, the E–W trending vein is richer in Ba, Zr, Th, and Pb, as well as poorer in U and F. Based on differentiation indexes such as the silica content or parameter B [Debon and Le Fort, 1983], the analysis referring to the major, minor, and trace elements did not reveal any clear evolutionary trends between the analyzed lithologies (Figure 6).

The REE spectra of the VPA and VNFC porphyries are illustrated in Figure 7a. Considering only the main facies of the veins, VNFC is the richest in REE, while PA is the poorest. The samples representing the aphyric facies of the VNFC specimen are strongly depleted, as is the compact lithology spatially associated with the PA porphyry. All REE spectra present a weak general fractionation, an LREE fractionation slightly more significant than the HREE fractionation, and negative, well-accentuated Eu anomalies. Overall, the VPA specimens are more homogeneous than the VNFC samples concerning the general REE fractionation (the difference is mainly due to the LREE). The Eu anomalies are more evident on the VPA profiles, especially on the ones illustrating the compact lithology. In the aphyric VNFC vein, the Eu anomalies are also clear.

Multi-element spidergrams of the VPA and VNFC porphyries are presented in Figure 7b. The patterns for both VPA veins and the compact facies exhibit identical anomalies, which are always more pronounced in the PA specimen and compact rock profiles. All spidergrams, including those representing the VNFC porphyry, present clear positive anomalies in HFSE such as U and Ta, as well as in Cs, P, and Pb, and evident negative anomalies in LILE like Ba and Sr. Titanium, niobium, and LREE anomalies are also negative. Regarding the VNFC vein, both the positive and negative anomalies are more pronounced in the profiles of the aphyric facies. As the REE spectra, the normalized multi-element spidergrams of the VPA subvolcanic lithologies also display parallel patterns.

4.3. *Sm–Nd isotope geochemistry*

Three samples of each porphyry were selected to study the respective Sm–Nd isotope systems.

Table 2. Sm and Nd isotopic composition of the Vila Pouca de Aguiar and Vila Nova de Foz Côa porphyries

Samples	Nd (ppm)	Sm (ppm)	$^{147}Sm/^{144}Nd$	$^{143}Nd/^{144}Nd \pm 2\sigma$	$\varepsilon Nd^{290\ Ma}$
61-B	6.30	1.59	0.1530	0.512362 ± 0.000007	−3.76
61-1C	4.47	1.18	0.1595	0.512359 ± 0.000007	−4.07
D1	4.53	1.26	0.1684	0.512361 ± 0.000005	−4.36
61-2	8.01	2.17	0.1637	0.512361 ± 0.000004	−4.19
61-2A	8.02	2.26	0.1707	0.512380 ± 0.000004	−4.07
61-6C	7.85	2.07	0.1595	0.512359 ± 0.000006	−4.07
VNFC1	13.7	3.07	0.1354	0.512296 ± 0.000006	−4.40
VNFC3A	12.3	2.48	0.1216	0.512277 ± 0.000006	−4.26
VNFC5	14.6	3.24	0.1342	0.512305 ± 0.000006	−4.18

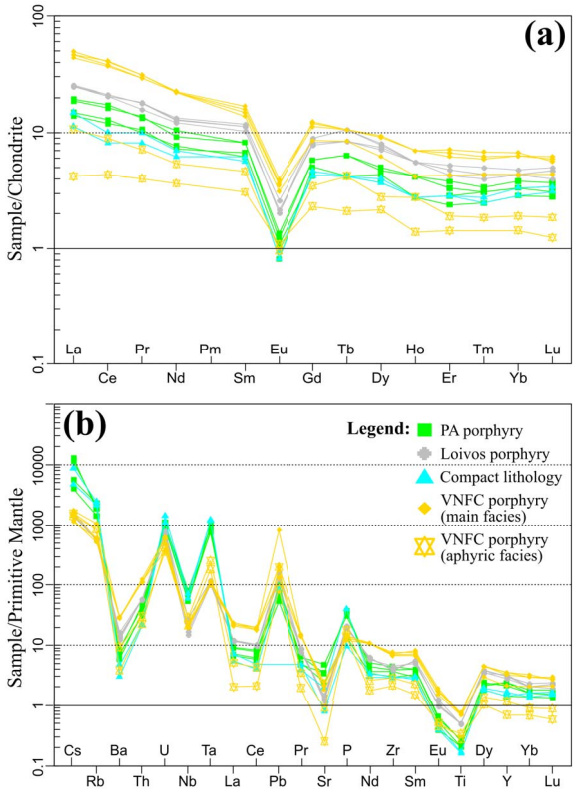

Figure 7. (a) REE diagrams for the VPA and VNFC porphyries. Chondrite normalization values after Boynton [1984]; (b) Multi-element spidergrams for the VPA and VNFC porphyries. Primitive mantle normalization values after McDonough and Sun [1995].

The results are presented in Table 2. To calculate the εNd_i parameter, a crystallization age of 290 Ma, which is the age of the youngest post-D_3 Variscan granites in Iberia, has been assumed. Overall, the VPA and VNFC veins exhibit similar isotopic compositions, with $\varepsilon Nd^{290\ Ma} = -3.76$ to -4.40. The Loivos and VNFC porphyries are relatively homogeneous, while the PA vein displays a wider range of initial εNd values. On average, the VPA specimens are more radiogenic in Nd than the VNFC porphyry.

5. Discussion

5.1. *Petrogenesis and relationship with the granites*

Several criteria suggest that the two porphyries of the VPA region are genetically related to each other. Both veins are N–S trending, the distance between them is regionally insignificant, and their mineral and bulk-rock geochemical compositions are very similar. As mentioned before, the third phase of the Variscan orogeny (D_3) was responsible for the development of conjugated, NNE–SSW and NNW–SSE trending, brittle fracture systems. The emplacement of the VPA porphyries was most likely controlled by similar structures, which were generated during the late stages of phase D_3 and superimposed by the post-tectonic D_4 brittle phase [Dias et al., 2013]. However, since the kinematic evolution of many of these fractures is polyphasic and associated with both late-Variscan and Alpine events [Mateus and Noronha, 2010], without geochronological results there is no

definitive confirmation that the generation and emplacement of the VPA porphyries were related to the final contributions of the Variscan orogeny or the onset of the Alpine tectonics in northern Iberia. The presence of scarce magmatic to submagmatic microstructures such as kinks and weak undulatory extinction [Bouchez et al., 1992] favors the former hypothesis because there is no record of folding or ductile shearing on northern Portugal caused by the Alpine cycle [Jabaloy Sánchez et al., 2019]. On the other hand, the VNFC porphyry was emplaced along a WSW–ENE ductile shear zone. According to Silva and Ribeiro [1991], this structure also resulted from the onset of phase D_3 on the portuguese CIZ. However, given the general orientation, the ductile shear was developed before the fractures where the VPA porphyries have emplaced [Dias et al., 2013]. As such, the regional structures and vein directions suggest that the emplacement of the VNFC porphyry took place before the emplacement of the VPA veins.

The main geochemical arguments in favor of a genetic relationship between the Loivos and PA porphyries are the parallel REE spectra and closeness of the $\varepsilon Nd^{290\ Ma}$ values. The small differences between the two VPA veins could be related to variations concerning the partial melting of the protolith and/or to the separate evolution of corresponding individual magma batches. Since the REE spidergrams of the compact lithology spatially associated with the PA porphyry are also parallel, this lithotype is probably a different facies of the eastern vein without phenocrysts, thus explaining the great similarities respecting mineralogy, texture, and geochemistry. The occurrence of the aphyric PA facies next to the GTMZ quartzphyllites and of a microgranite in the contact between the VPA granite and Loivos porphyry suggests that these lithologies represent a sharp thermal transition or chilled margins between the veins and respective host rocks. The same can be noted about the VNFC porphyry, whose aphyric facies probably constitutes a chilled margin at the contact with the regional host rocks (i.e., mainly syn-D_3 granites). In the PA and VNFC cases, the higher thermal contrast between the porphyries and respective host rocks created microcrystalline, subvolcanic to volcanic textures. On the other hand, in Loivos, since the vein completely intruded into a post-D_3 granite (which was warmer at the time of emplacement), the resulting transition is more phaneritic.

The highly evolved nature of the porphyries suggests that the melts from which they crystallized were subjected to crystal fractionation. The strong negative Eu anomalies possibly point to plagioclase fractionation in the source, without discarding possible inheritance from the protolith, while the $(La/Sm)_N$ ratios and low Zr + Hf + Y + Th contents are related to the crystal fractionation of apatite, zircon, allanite, and monazite [Zhu and O'Nions, 1999]. As mentioned above, the REE spectra of the aphyric facies are parallel to the spectra of the porphyritic ones. Petrographically, the lack of phenocrysts and the absence of most accessory minerals in the aphyric varieties are directly related to the compositional differences between the two types of facies. Overall, the whole-rock geochemical data indicate that the PA porphyry is more fractionated than the Loivos vein. The previous statement is evidenced by multiple geochemical observations namely the following: (i) the higher $Fe_2O_3^t$, MgO, and TiO_2 contents in Loivos, which are related to the greater amount of biotite and other ferromagnesian minerals (e.g. ilmenite); (ii) the higher Nb and Ta, and lower Ba and Zr contents of the PA porphyry; (iii) the average weaker general REE fractionation of the PA vein; (iv) the less pronounced anomalies in the multi-element spidergrams of the Loivos lithotype; and (v) the geochemical and geotectonic classifications as illustrated in Figure 5. However, the higher SiO_2 and K_2O contents of the Loivos porphyry contrast with the aforementioned interpretations. The intense hydrothermal alterations that affected the PA vein are the probable causes [Maia et al., 2014, Ballouard et al., 2016a]. Following the same criteria, the VNFC porphyry is the least evolved one. The particularly high silica and alumina contents of the aphyric facies that cause samples VNFC2B and 3B to be plotted outside the regular diagram ranges are reflected in the mineral assemblage, which is almost solely dominated by quartz and microcrystalline muscovite. These rocks possibly represent a very evolved residual melt, tending to shift toward silica-rich hydrothermal fluids. Considering the geochemical features displayed by sample VNFC3A, the latter behaves similarly to the aphyric facies, implying a strong hydrothermal influence.

Considering the geochemical and isotope data of the regional Variscan granites [εNd_i [VPA granite] = −2.47 to −2.54; Martins et al., 2009; εNd_i [VNFC granites] = −6.03 to −8.89; Ferreira et al., 2020], our

results suggest that the sources from which the porphyries derived are different compared to those from which the granites were generated. The average bulk-rock compositions and geochemical classifications of the least altered samples point out the higher evolutionary degree of the subvolcanic rocks. The enrichment in rare incompatible metal elements is most likely associated with fractionation of a feldspar and biotite-dominated assemblage, generating high contents in LILE such as Li, Be, Rb, and Cs [Canosa et al., 2012, Simons et al., 2017]. As the magmatic system evolved, the residual melts from which the porphyries crystallized became enriched in the latter elements, as well as in Sn, Nb, Ta, and W, due to their highly incompatible behavior. In the veins, the LILE were probably partitioned into muscovite and K-feldspar through the substitution of K [Canosa et al., 2012]. On the other hand, the high P_2O_5 and F contents promoted the retention of HFSE (Sn, Nb, Ta, W) in the porphyry melts [Simons et al., 2017], resulting in their partition into Fe and Ti oxides (ilmenite and, to a lesser extent, biotite), Nb and Ta oxides (columbite–tantalite), and Sn oxides (cassiterite), as verified with the SEM-EDS analysis. Since tungsten is preferentially incorporated into muscovite in granitic melts of lower temperature [Simons et al., 2017], the veins also became enriched over the granites.

As previously mentioned, the studied porphyries resemble "A-type" granitoids which is mostly evidenced by their high HFSE and F contents, elevated Ga/Al ratio, post-orogenic signatures, and presence of rare phosphates [Whalen et al., 1987, Bonin, 2007]. Several theories have been proposed to explain the petrogenesis of this controversial group of igneous rocks [e.g. Bonin, 2007, Magna et al., 2010, Sarjoughian et al., 2015, and references therein]. The main petrogenetic models are summarized in the following list: (i) remelting of a granulitic residue that was left in the lower crust after a previous extraction of "I-type" granite melts; (ii) anatexis of quartzofeldspathic (meta)igneous crustal rocks; (iii) mixing of magmas derived from crustal and OIB sources; (iv) significant crystal fractionation of mantle-derived mafic melts; (v) generation from a depleted upper mantle reservoir altered by subduction-related fluids; and (vi) anatexis of a lower crustal source, previously metasomatized by mantle-derived fluids. Considering the peraluminous nature of the veins, the low Zr and REE contents, the lack of alkali-rich amphiboles and/or sodic pyroxenes, and the absence of significant volumes of alkaline rocks near the porphyry outcrops, the last three models are refuted [Martin, 2006, Bonin, 2007]. On the other hand, the granulitic residue remelting scenario is excluded due to the enriched nature of the VPA pluton [Martins et al., 2009]. If the veins had been generated from such a residue, their contents in rare incompatible metal elements would be lower than those of the granites. In the multi-element spidergrams, the anomalies revealed by the VPA and VNFC porphyries imply that the magmas from which the veins crystallized must have been derived from evolved crustal sources [Nédélec and Bouchez, 2015]. The evolved nature of the porphyry sources is also evidenced by the weakly fractionated REE spectra [Wu et al., 2017]. However, considering the Nd isotope signatures, magma mixing might have occurred. As such, the likeliest petrogenetic model is the anatexis of quartzofeldspathic crustal rocks under reducing conditions (since the magnetic mineralogy is dominated by ilmenite and biotite), with probable influence of compositionally different melts, followed by significant crystal fractionation.

The REE spectra of the aphyric facies are slightly arcuate in the profiles of both LREE and HREE (especially in the case of VNFC), reflecting the REE tetrad effect [Peppard et al., 1969, Irber, 1999] generated from hydrothermal influences (under magmatic to hydrothermal subsolidus conditions as proposed by Ballouard et al. [2016a]). The stronger rubefaction in the PA vein highlights the higher degree of hydrothermalism. Geochemically, the low K/Rb and Nb/Ta ratios also point out the severe hydrothermal alterations (Loivos: $128.65 < K/Rb < 141.39$; $2.68 < Nb/Ta < 4.09$; PA: $26.64 < K/Rb < 44.28$; $0.90 < Nb/Ta < 1.61$; VNFC: $66.97 < K/Rb < 122.62$; $2.00 < Nb/Ta < 3.51$) and suggest that crystal fractionation of biotite and ilmenite have played an important role in the geochemical evolution of the porphyries [Ballouard et al., 2016a,b, 2020]. Since these alterations seem to have been caused by F-rich fluids, some apatite and the rare phosphates of the VPA veins possibly resulted from the transformation of P-rich alkali feldspars [Bea et al., 1992, Broska et al., 2004]. On the other hand, post-magmatic processes have affected the geochemistry of the aphyric samples and are presumably responsible for the depletion in Na_2O [Förster et al., 2007]. Due to these phenomena, the

K_2O and Rb contents of the phenocryst-free samples may also be lower than in the unaltered ones, thus generating a less alkalic nature.

5.2. *Texture development*

The generation of porphyritic aphanitic textures in volcanic and subvolcanic rocks of rhyolitic/granitic composition is mainly explained by magmatic histories involving two separate melt cooling episodes [Best and Christiansen, 2001]. The first episode is associated with a slow cooling rate and small undercooling, resulting in large phenocrysts of variable size. Phenocryst growth typically occurs deep below the surface in magmatic reservoirs. On the other hand, the second cooling episode takes place at shallow depths after a rapid heat loss. The fast cooling, combined with a large nucleation rate and low growth rate, explains the multiple finer crystals that compose the aphanitic groundmass. However, there are other theories about the development of this type of igneous texture, such as a single, long, continuous cooling event where the first mineral to precipitate from the liquidus crystallizes alone for a long period of time, causing strong supersaturations in the melt [Vernon, 2004]. Another widely recognized and accepted theory involves two stages of fluid saturation. The initial phenocryst nucleation and growth are promoted by a first stage of volatile supersaturation, while the second stage takes place after isothermal decompression and devolatilization of the melt. This hypothesis is more suited to explain the bimodal granularity of porphyry masses [Ferreira and Ribeiro, 2018]. Considering the textural variety displayed by the VPA and VNFC porphyries, both fast cooling and volatile loss have probably played a crucial role.

All studied porphyries exhibit three different grain size populations: (i) the earlier phenocrysts and microphenocrysts; (ii) the coarser groundmass grains; and (iii) the finer groundmass crystals. Assuming that the phenocrysts and microphenocrysts were generated in conditions of fluid supersaturation, the presence of embayments in quartz [formed from resorption or dendritic growth; Barbey et al., 2019, Barbee et al., 2020] and the micrographic intergrowths (granophyric texture) constitute an indirect evidence of varying cooling rates and undercooling magnitude [Štemprok et al., 2008]. Since the porphyries occur as veins, a rapid (and nearly isothermal) magma ascent is presumed. Isothermal decompression can lead to the partial resorption of quartz and feldspar, until fluid saturation conditions are reached, resulting in a melt fraction increase and the development of embayments. Under fluid-saturated conditions, quartz may undergo renewed growth, and novel plagioclase and K-feldspar crystallization is possible [Štemprok et al., 2008]. If the novel feldspar crystallization is epitactic, rapakivi and antirapakivi feldspars can be formed [Nekvasil, 1991, Corretgé and Suárez, 1994]. As the decompression progresses, the melt is increasingly cooled due to the rapid heat transfer onto the host rocks, triggering a significant devolatilization and crystallization of the residual melt in very fine groundmass grains. The groundmass crystals (or microliths) formed through this process are commonly arranged around the phenocrysts [Ferreira and Ribeiro, 2018]. At shallow emplacement levels, cooling rates for the porphyry melts are expected to be high. However, in the case of the Loivos porphyry, since the vein is completely hosted in a post-D_3 granite, which was warmer at the time of emplacement, the cooling rate may have been lower. As such, it is possible to presume that the coarser groundmass grains resulted from subsolidus annealing which coarsened and partially eliminated the finer groundmass [Higgins, 1999, 2000, Štemprok et al., 2008]. On the other hand, the PA porphyry was emplaced closer to the edge of the VPA pluton, next to metasedimentary rocks, and the VNFC vein is hosted in colder syn-D_3 granites and metasediments. In these cases, at the time of porphyry emplacement, the thermal contrast was more significant, and the groundmass coarsening was presumably hindered.

5.3. *Antirapakivi and rapakivi feldspars*

Various theories have been proposed to explain the generation of rapakivi and antirapakivi feldspars in plutonic, subvolcanic, and volcanic settings. The two most accepted hypotheses are based on isothermal decompression of granitic melts [Nekvasil, 1991, Corretgé and Suárez, 1994] and mixing or mingling of two compositionally distinct magmas [Abbott, 1978, Hibbard, 1981, Stimac and Wark, 1992, Wark and Stimac, 1992, Andersson and Eklund, 1994, Müller and Seltmann, 2002, Seltmann and Müller, 2002, Müller et al., 2005, 2008, O'Brien et al., 2019]. Some authors believe that both phenomena are crucial in the

development of rapakivi textures, although attributing greater importance to the magma mixing [Rämö and Haapala, 1995, Vernon, 2016]. Other (and less recognized) models such as synneusis [Stull, 1979] and subsolidus exsolution [Dempster et al., 1994] have been refuted.

The discrimination of the contributions of magma mixing and isothermal decompression on the development of mantled feldspars in individual intrusions is very difficult [Vernon, 2016]. As mentioned above, the groundmass crystals arranged around the phenocrysts, the embayments on quartz and K-feldspar phenocrysts, and the granophyric texture collectively suggest that the porphyry melts were subjected to devolatilization and isothermal decompression. Geochemically, the high variability of all porphyries regarding their fluorine contents constitutes another argument in favor of variable undercooling rates and volatile loss [Boyle, 1976, Bailey, 1977]. However, the influence of magma mixing should not be discarded, especially in high-level intrusions such as granite porphyries. Concerning the VPA and VNFC veins, the only feature that is undeniably related to mixing of two compositionally distinct magmas is the coexistence of mantled and non-mantled feldspar phenocrysts [Vernon, 2016].

Rämö and Haapala [1995] stated that most granites exhibiting rapakivi texture are associated with mafic rocks such as gabbros, norites, anorthosites, dolerites, and basalts, which represent the mafic member of the bimodal magmatism typically associated with rapakivi suites. While in VPA there are no such lithologies in the vicinities of the porphyries, in the VNFC region there are multiple small microgabbro veins close to the regional porphyry. These microgabbros are, like the porphyry, emplaced along late to post-D_3 structures. Geochemically, the three granitic veins present some characteristics typical of rapakivi granites, namely the high SiO_2, F, K_2O, Rb, Th, and U, and low CaO, MgO, and Sr contents, and the post-orogenic signature. In the case of magma mixing, the development of the rapakivi/antirapakivi textures should have occurred in the deeper magma reservoir where the phenocrysts were formed. On the other hand, if the mantled feldspars were generated during decompression, they formed during the ascent of the magmas along the veins. Considering the results presented in this work, both magma mixing and isothermal decompression may be regarded as the phenomena responsible for the petrographic, textural, and geochemical evolution of the VPA and VNFC porphyries.

6. Conclusions

The Vila Pouca de Aguiar and Vila Nova de Foz Côa porphyries are three of the most regionally significant subvolcanic veins of northern Portugal and portuguese Central Iberian Zone. The following interpretations were reached based on field, petrographic, textural, SEM-EDS, whole-rock geochemical, and Sm–Nd isotope studies:

(1) Considering their geometry, spatial proximity, mineral assemblages, and bulk-rock chemical compositions, the Loivos and Póvoa de Agrações porphyries of the VPA region are possibly genetically related to each other. Despite its less evolved nature, the VNFC vein presumably derived from a similar source;

(2) All of the studied porphyries were emplaced along structures generated during the final phase of the Variscan orogeny and reactivated with the Alpine cycle. The presence of magmatic to submagmatic microstructures suggests that porphyry emplacement occurred toward the end of the Variscan orogeny. Based on the general vein orientation, the VPA subvolcanics are probably (slightly) younger than the VNFC counterpart;

(3) Both the PA and VNFC porphyries exhibit two facies, the main porphyritic one, and the other, practically phenocryst-free, and aphyric. The aphyric facies and the microgranite that is spatially associated with the Loivos vein are chilled margins or transitional lithologies between the main porphyritic facies and the respective regional host rocks. The textural differences between these lithologies are related to the magnitude of the thermal contrasts at the time of emplacement;

(4) The likeliest petrogenetic model is the anatexis of quartzofeldspathic crustal rocks, under reducing conditions, seemingly influenced by compositionally different melts resulting in magma mixing, followed by significant crystal fractionation. Based on the geochemical data, the sources from which the regional granites were generated are not the same;

(5) The three veins were significantly affected by subsolidus hydrothermal fluids, as indicated by several petrographic and geochemical evidence, namely

rubefaction, the presence of rare phosphates, low K/Rb and Nb/Ta ratios, and the REE tetrad effect;

(6) All porphyries are enriched in rare metal incompatible elements. SEM-EDS analyses showed that some of these metals (Nb, Ta, Sn) are concentrated in various oxides (ilmenite, brookite, anatase, columbite–tantalite, cassiterite). The remaining elements (Li, Be, Rb, Cs, W) are probably incorporated in muscovite and K-feldspar. Despite the small distance separating the VPA veins, Póvoa de Agrações is significantly richer in all of these elements, which is possibly due to both crystal fractionation and hydrothermalism;

(7) The textural evolution of the VPA and VNFC porphyries was probably conditioned by fast cooling, volatile loss, and subsolidus annealing. Presumably, the latter process preferentially affected the Loivos vein;

(8) Based on the results of this research, both isothermal decompression and magma mixing are likely to have played an important role in the petrogenesis of the studied porphyries.

Further investigation, such as geochronology and more isotope studies, is required to fully understand the differences between these porphyries and to improve the current state of knowledge regarding the felsic vein magmatism in northern Portugal.

Conflicts of interest

Authors have no conflict of interest to declare.

Acknowledgments

This work was supported by the Fundação para a Ciência e Tecnologia (FCT), through the project reference UIDB/04683/2020—ICT (Institute of Earth Sciences). The corresponding author is also financially supported by FCT through an individual PhD grant (reference SFRH/BD/138818/2018). The authors thank Professor Fernando Noronha (ICT, Porto Pole) for his help during the field studies, Daniela Silva (CEMUP) for her assistance throughout the SEM-EDS sessions, and Dr. Javier Rodríguez (SGIKER, University of the Basque Country) for the isotopic analyses. We also acknowledge Professor Pierre Barbey, an anonymous reviewer, and editor Bruno Scaillet whose comments helped to greatly improve the quality of the original manuscript.

Appendix A. Geographic coordinates of the sampling sites (coordinate system: Lisboa Hayford Gauss IGeoE)

Samples	Location	Lithology	Latitude	Longitude
61-1	VPA	PA porphyry	N 41° 36′ 28″	W 7° 29′ 24″
61-1C	VPA	PA porphyry	N 41° 36′ 28″	W 7° 29′ 24″
61-B	VPA	PA porphyry	N 41° 37′ 32″	W 7° 29′ 56″
D1	VPA	PA porphyry	N 41° 37′ 58″	W 7° 29′ 21″
61-2	VPA	Loivos porphyry	N 41° 36′ 31″	W 7° 30′ 24″
61-2A	VPA	Loivos porphyry	N 41° 37′ 27″	W 7° 30′ 16″
61-6Ca	VPA	Loivos porphyry	N 41° 35′ 52″	W 7° 32′ 22″
61-6Cb	VPA	Loivos porphyry	N 41° 35′ 52″	W 7° 32′ 22″
Micro	VPA	Microgranite	N 41° 37′ 45″	W 7° 30′ 18″
CC green	VPA	Compact lithology	N 41° 37′ 58″	W 7° 29′ 21″
CC pink	VPA	Compact lithology	N 41° 36′ 28″	W 7° 29′ 24″
VNFC1	VNFC	VNFC porphyry (main facies)	N 40° 59′ 35″	W 7° 9′ 58″
VNFC2A	VNFC	VNFC porphyry (main facies)	N 40° 59′ 38″	W 7° 9′ 57″
VNFC2B	VNFC	VNFC porphyry (aphyric facies)	N 40° 59′ 38″	W 7° 9′ 57″
VNFC3A	VNFC	VNFC porphyry (main facies)	N 40° 59′ 37.7″	W 7° 9′ 48.5″
VNFC3B	VNFC	VNFC porphyry (aphyric facies)	N 40° 59′ 37.7″	W 7° 9′ 48.5″
VNFC5	VNFC	VNFC porphyry (main facies)	N 40° 59′ 17.3″	W 7° 8′ 13.4″

Appendix B. Specifications on the SEM-EDS analysis

Polished thin sections of the VPA porphyries were analyzed through scanning electron microscopy coupled with energy-dispersive X-ray spectroscopy (SEM-EDS). SEM-EDS usage was deemed necessary due to the extremely fine granularity that these subvolcanic rocks exhibit. This analytical methodology was also crucial in the identification of certain unusual minerals. Selected samples were examined at the IMICROS laboratory, CEMUP (Imaging, Microstructure, and Microanalysis Unit of the Materials Center, Porto University), using a high-resolution scanning electron microscope with X-ray microanalysis: model JEOL JSM 6301F/Oxford INCA Energy 350. All analyzed samples were previously coated by vapor deposition with a fine carbon film, using a JEOL JEE-4X Vacuum Evaporator equipment. The conditions in which the X-ray spectra were obtained are the following: accelerating voltage—15 kV; work distance (WD)—15 mm. The detection limit for all elements (from boron to uranium) is 0.1%.

References

Abbott, R. N. (1978). Peritectic reactions in the system An-Ab-Or-Qz-H_2O. *Can. Mineral.*, 16(2), 245–256.

Alasino, P. H., Dahlquist, J. A., Galindo, C., Baldo, E. G., and Casquet, C. (2004). Granitoides peraluminosos con andalucita y cordierita magmáticas en la sierra de Velasco: implicancias para el orógeno famatiniano. *Asoc. Geol. Argent. D: Publ. Espec.*, (8), 109–122.

Alibert, C. (1985). A Sr–Nd isotope and REE study of late Triassic dolerites from the Pyrenees (France) and the Messejana Dyke (Spain and Portugal). *Earth Planet. Sci. Lett.*, 73, 81–90.

American Geological Institute (1962). *Dictionary of Geological Terms*. Dolphin Books Inc., New York, United States.

Andersson, U. B. and Eklund, O. (1994). Cellular plagioclase intergrowths as a result of crystal-magma mixing in the Proterozoic Åland rapakivi batholith, SW Finland. *Contrib. Mineral. Petrol.*, 117(2), 124–136.

Azevedo, M. R. and Valle Aguado, B. (2013). Origem e Instalação de Granitóides Variscos na Zona Centro-Ibérica. In Dias, R., Araújo, A., Terrinha, P., and Kullberg, J. C., editors, *Geologia de Portugal*, volume I of *Geologia Pré-mesozóica de Portugal*, pages 377–401. Escolar Editora, Lisbon, Portugal.

Bailey, J. C. (1977). Fluorine in granitic rocks and melts: a review. *Chem. Geol.*, 19(1–4), 1–42.

Ballouard, C., Branquet, Y., Tartèse, R., Poujol, M., Boulvais, P., and Vigneresse, J. L. (2016b). Nb–Ta fractionation in peraluminous granites: A marker of the magmatic-hydrothermal transition: REPLY. *Geology*, 44(7), article no. e395.

Ballouard, C., Massuyeau, M., Elburg, M. A., Tappe, S., Viljoen, F., and Brandenburg, J. T. (2020). The magmatic and magmatic-hydrothermal evolution of felsic igneous rocks as seen through Nb-Ta geochemical fractionation, with implications for the origins of rare-metal mineralizations. *Earth-Sci. Rev.*, 203, article no. 103115.

Ballouard, C., Poujol, M., Boulvais, P., Branquet, Y., Tartèse, R., and Vigneresse, J. L. (2016a). Nb–Ta fractionation in peraluminous granites: A marker of the magmatic-hydrothermal transition. *Geology*, 44(3), 231–234.

Barbee, O., Chesner, C., and Deering, C. (2020). Quartz crystals in Toba rhyolites show textures symptomatic of rapid crystallization. *Am. Mineral.: J. Earth Planet. Mater.*, 105(2), 194–226.

Barbey, P., Faure, F., Paquette, J. L., Pistre, K., Delangle, C., and Gremilliet, J. P. (2019). Skeletal quartz and dendritic biotite: Witnesses of primary disequilibrium growth textures in an alkali-feldspar granite. *Lithos*, 348–349, article no. 105202.

Barnard, K. R., McDonald, R. G., Pownceby, M. I., Sparrow, G. J., and Zhang, W. (2019). Processing anatase ores for pigment production. *Hydrometallurgy*, 185, 226–237.

Bea, F., Fershtater, G., and Corretgé, L. G. (1992). The geochemistry of phosphorus in granite rocks and the effect of aluminium. *Lithos*, 29(1–2), 43–56.

Bea, F., Montero, P., and Molina, J. F. (1999). Mafic precursors, peraluminous granitoids, and late lamprophyres in the avila batholith: A model for the generation of variscan batholiths in Iberia. *J. Geol.*, 107(4), 399–419.

Best, M. G. and Christiansen, E. H. (2001). *Igneous Petrology*. Blackwell Science Ltd, London, England. ISBN: 0-86542-541-8.

Bonin, B. (2004). Do coeval mafic and felsic magmas in post-collisional to within-plate regimes necessarily imply two contrasting, mantle and crustal, sources? A review. *Lithos*, 78(1–2), 1–24.

Bonin, B. (2007). A-type granites and related rocks: Evolution of a concept, problems and prospects. *Lithos*, 97(1–2), 1–29.

Bouchez, J. L., Delas, C., Gleizes, G., Nédélec, A., and Cuney, M. (1992). Submagmatic microfractures in granites. *Geology*, 20(1), 35–38.

Boyle, D. R. (1976). *The geochemistry of fluorine and its applications in mineral exploration.* PhD thesis, University of London.

Boynton, W. V. (1984). Geochemistry of the rare earth elements: meteorite studies. In Henderson, P., editor, *Rare Earth Element Geochemistry*, pages 63–114. Elsevier, Amsterdam, Netherlands.

Broska, I., Williams, C. T., Uher, P., Konečný, P., and Leichmann, J. (2004). The geochemistry of phosphorus in different granite suites of the Western Carpathians, Slovakia: the role of apatite and P-bearing feldspar. *Chem. Geol.*, 205(1–2), 1–15.

Cabanis, B. and Lecolle, M. (1989). Le diagramme La/10-Y/15-Nb/8: un outil pour la discrimination des séries volcaniques et la mise en évidence des processus de mélange et/ou de contamination crustale. *C. R. Acad. Série 2, Méc. Phys. Chim. Sci. Sci. Terre*, 309(20), 2023–2029.

Canosa, F., Martin-Izard, A., and Fuertes-Fuente, M. (2012). Evolved granitic systems as a source of rare-element deposits: the Ponte Segade case (Galicia, NW Spain). *Lithos*, 153, 165–176.

Corretgé, L. G. and Suárez, O. (1994). A garnet-cordierite granite porphyry containing rapakivi feldspars in the cabeza de araya batholith (extremadura, Spanish Hercynian belt). *Mineral. Petrol.*, 50(1–3), 97–111.

Cruz, C. C. F. (2020). *Post-tectonic Variscan magmatism from northwest Iberia. Implications for W-Mo metallogeny. Case study of Lamas de Olo Pluton.* PhD thesis, Universidade do Porto.

Damian, F., Damian, G., and Constantina, C. (2009). The subvolcanic magmatic rocks from the Nistru zone (Gutîi Mountains). *Carpathian J. Earth Environ. Sci.*, 4(2), 101–122.

De La Roche, H., Leterrier, J., Grandclaude, P., and Marchal, M. (1980). A classification of volcanic and plutonic rocks using R1–R2 diagrams and major element analysis — its relationships with current nomenclature. *Chem. Geol.*, 29(1–4), 183–210.

Debon, F. and Le Fort, P. (1983). A chemical-mineralogical classification of common plutonic rocks and associations. *Earth Environ. Sci. Trans. R. Soc. Edinburgh*, 73(3), 135–149.

Dempster, T. J., Jenkin, G. R. T., and Rogers, G. (1994). The origin of rapakivi texture. *J. Petrol.*, 35(4), 963–981.

Dias, G., Noronha, F., Almeida, A., Simões, P. P., Martins, H. C. B., and Ferreira, N. (2010). Geocronologia e petrogénese do plutonismo tardi-varisco (NW de Portugal): síntese e inferências sobre os processos de acreção e reciclagem crustal na Zona Centro-Ibérica. In Cotelo Neiva, J. M., Ribeiro, A., Mendes Victor, L., Noronha, F., and Magalhães Ramalho, M., editors, *Ciências Geológicas: Ensino, Investigação e sua História*, volume I of *Geologia Clássica*, pages 143–160. Associação Portuguesa de Geólogos, Lisbon, Portugal.

Dias, R. and Ribeiro, A. (1995). The Ibero-Armorican Arc: a collisional effect against an irregular continent? *Tectonophysics*, 246(1–3), 13–128.

Dias, R., Ribeiro, A., Coke, C., Pereira, E., Rodrigues, J., Castro, P., Moreira, N., and Rebelo, J. (2013). Evolução estrutural dos sectores setentrionais do Autóctone da Zona Centro-Ibérica. In Dias, R., Araújo, A., Terrinha, P., and Kullberg, J. C., editors, *Geologia de Portugal*, volume I of *Geologia Pré-mesozóica de Portugal*, pages 73–147. Escolar Editora, Lisbon, Portugal.

Dias, R., Ribeiro, A., Romão, J., Coke, C., and Moreira, N. (2016). A review of the arcuate structures in the Iberian Variscides; constraints and genetic models. *Tectonophysics*, 681, 170–194.

Ferreira, J. A., Mata, J., Bento dos Santos, T., and Pereira, I. (2020). The role of melting on the geochemical evolution and isotopic variability of an anatectic complex in the Iberian Variscides. *Lithos*, 378–379, article no. 105769.

Ferreira, N., Iglésias, M., Noronha, F., Ribeiro, A., and Ribeiro, M. L. (1987). Granitóides da Zona Centro Ibérica e seu enquadramento geodinâmico. In Bea, F., Carnicero, A., Gonzalo, J. C., López Plaza, M., and Rodriguez Alonso, M. D., editors, *Geologia de los Granitoides e Rocas Asociadas del Macizo Hespérico*, pages 37–51. Editorial Rueda, Madrid, Spain.

Ferreira, P. and Ribeiro, M. A. (2018). Estudo petrográfico e geoquímico do granito de Bagunte e pórfiro associado. *Comun. Geol.*, 105(1), 45–55. ISSN: 0873-948X; e-ISSN: 1647-581X.

Förster, H. J., Gottesmann, B., Tischendorf, G., Siebel, W., Rhede, D., Seltmann, R., and Wasternack, J.

(2007). Permo–Carboniferous subvolcanic rhyolitic dikes in the western Erzgebirge/Vogtland, Germany: a record of source heterogeneity of post-collisional felsic magmatism. *Neues Jahrb. für Mineral.-Abhandlungen: J. Mineral. Geochem.*, 183(2), 123–147.

Frost, B. R., Barnes, C. G., Collins, W. J., Arculus, R. J., Ellis, D. J., and Frost, C. D. (2001). A geochemical classification for granitic rocks. *J. Petrol.*, 42(11), 2033–2048.

Hibbard, M. J. (1981). The magma mixing origin of mantled feldspars. *Contrib. Mineral. Petrol.*, 76(2), 158–170.

Higgins, M. D. (1999). Origin of megacrysts in granitoids by textural coarsening: a crystal size distribution (CSD) study of microcline in the Cathedral Peak Granodiorite, Sierra Nevada, California. In *Geological Society, London, Special Publications 168*, pages 207–219. Geological Society, London, UK.

Higgins, M. D. (2000). Measurements of crystal size distributions. *Am. Mineral.*, 85(9), 1105–1116.

Irber, W. (1999). The lanthanide tetrad effect and its correlation with K/Rb, Eu/Eu*, Sr/Eu, Y/Ho, and Zr/Hf of evolving peraluminous granite suites. *Geochim. Cosmochim. Acta*, 63(3/4), 489–508.

Jabaloy Sánchez, A., Padrón-Navarta, J. A., Gómez-Pugnaire, M. T., López Sánchez-Vizcaíno, V., and Garrido, C. J. (2019). Alpine Orogeny: Deformation and Structure in the Southern Iberian Margin (Betics s.l.). In Quesada, C. and Oliveira, J., editors, *The Geology of Iberia: A Geodynamic Approach, Volume 3: The Alpine Cycle*, Regional Geology Reviews, pages 453–486. Springer, Cham, Switzerland.

Jacobsen, S. B. and Wasserburg, G. J. (1984). Sm–Nd isotopic evolution of chondrites and achondrites, II. *Earth Planet. Sci. Lett.*, 67(2), 137–150.

Jokela, E. (2020). Geology, geochemistry and metamorphic petrology of the Sukseton area, Kittilä, Central Lapland Greenstone Belt, Finland. Master's thesis, University of Helsinki.

Lugmair, G. W. and Marti, K. (1978). Lunar initial $^{143}Nd/^{144}Nd$: Differential evolution of the lunar crust and mantle. *Earth Planet. Sci. Lett.*, 39(3), 349–357.

Magna, T., Janoušek, V., Kohút, M., Oberli, F., and Wiechert, U. (2010). Fingerprinting sources of orogenic plutonic rocks from Variscan belt with lithium isotopes and possible link to subduction-related origin of some A-type granites. *Chem. Geol.*, 274(1–2), 94–107.

Maia, M., Jaques, L., Bobos, I., and Noronha, F. (2014). Estudo mineralógico, petrográfico e geoquímico do processo pós-magmático do granito de Freixiosa-Mesquitela, Mangualde, Portugal: dados preliminares. *Comun. Geol.*, 101(1), 137–142.

Marques, F., Mateus, A., and Tassinari, C. (2002). The late-Variscan fault network in central-northern Portugal (NW Iberia): a re-evaluation. *Tectonophysics*, 359(3–4), 255–270.

Martin, R. F. (2006). A-type granites of crustal origin ultimately result from open-system fenitization-type reactions in an extensional environment. *Lithos*, 91(1–4), 125–136.

Martínez Catalán, J. R., Arenas, R., Abati, J., Sánchez Martínez, S., Díaz Garcia, F., Fernández Suárez, J., Cuadra, P. G., Castiñeiras, P., Gómez Barreiro, J., Díez Montes, A., González Clavijo, E., Rubio Pascual, F. J., Andonaegui, P., Jeffries, T. E., Alcock, J. E., Díez Fernández, R., and López Carmona, A. (2009). A rootless suture and the loss of the roots of a mountain chain: The Variscan belt of NW Ibéria. *C. R. Geosci.*, 341(2–3), 114–126.

Martins, H. C. B., Sant'Ovaia, H., and Noronha, F. (2009). Genesis and emplacement of felsic Variscan plutons within a deep crustal lineation, the Penacova-Régua-Verín fault: An integrated geophysics and geochemical study (NW Iberian Peninsula). *Lithos*, 111(3–4), 142–155.

Martins, H. C. B., Sant'Ovaia, H., and Noronha, F. (2013). Late-Variscan emplacement and genesis of the Vieira do Minho composite pluton, Central Iberian Zone: Constraints from U–Pb zircon geochronology, AMS data and Sr–Nd–O isotope geochemistry. *Lithos*, 162–163, 221–235.

Martins, H. C. B., Simões, P., and Abreu, J. (2014). Zircon crystal morphology and internal structures as a tool for constraining magma sources: Examples from northern Portugal Variscan biotite-rich granite plutons. *C. R. Geosci.*, 346(9–10), 233–243.

Mateus, A. and Noronha, F. (2010). Sistemas mineralizantes epigenéticos na Zona Centro-Ibérica; expressão da estruturação orogénica Meso-a Tardi-Varisca. In Cotelo Neiva, J. M., Ribeiro, A., Mendes Victor, L., Noronha, F., and Magalhães Ramalho, M., editors, *Ciências Geológicas: Ensino, Investigação e sua História*, volume 2 of *Geologia*

Aplicada, pages 47–62. Associação Portuguesa de Geólogos, Lisbon, Portugal.

McDonough, W. F. and Sun, S. S. (1995). The composition of the Earth. *Chem. Geol.*, 120(3–4), 223–253.

Müller, A., Breiter, K., Seltmann, R., and Pécskay, Z. (2005). Quartz and feldspar zoning in the eastern Erzgebirge volcano-plutonic complex (Germany, Czech Republic): evidence of multiple magma mixing. *Lithos*, 80(1–4), 201–227.

Müller, A. and Seltmann, R. (2002). Plagioclase-mantled K-feldspar in the Carboniferous porphyritic microgranite of Altenberg-Frauenstein, Eastern Erzgebirge/Krušné Hory. *Bull. Geol. Soc. Finland*, 74(1–2), 53–76.

Müller, A., Seltmann, R., Kober, B., Eklund, O., Jeffries, T., and Kronz, A. (2008). Compositional zoning of rapakivi feldspars and coexisting quartz phenocrysts. *Can. Mineral.*, 46(6), 1417–1442.

Nédélec, A. and Bouchez, J. L. (2015). *Granites: Petrology, Structure, Geological Setting, and Metallogeny*. Oxford University Press, Oxford, UK. ISBN: 978-0-19-870561-1.

Nekvasil, H. (1991). Ascent of felsic magmas and formation of rapakivi. *Am. Mineral.*, 76(7–8), 1279–1290.

Noronha, F., Ribeiro, M. A., Martins, H. C., and Lima, J. (1998). *Carta Geológica de Portugal na escala 1:50,000–folha 6-D–Vila Pouca de Aguiar*. Instituto Geológico e Mineiro, Lisbon, Portugal.

O'Brien, W. D., Dorais, M. J., Christiansen, E. H., and Gibson, D. (2019). Formation of rapakivi feldspar in the Deer Isle Granite Complex, coastal Maine: in situ lead isotope and trace-element analysis. *Contrib. Mineral. Petrol.*, 174, article no. 56.

Oliveira, A., Martins, H. C. B., and Sant'Ovaia, H. (2018). Estudo preliminar do pórfiro granítico de Vila Nova de Foz Côa: uma abordagem multidisciplinar. In *Livro de Atas do VIII Congresso Jovens Investigadores em Geociências, LEG 2018, Estremoz, 24–25 de novembro de 2018*, pages 173–177, Estremoz, Portugal. Pólo de Estremoz da Universidade de Évora.

Oliveira, A., Martins, H. C. B., and Sant'Ovaia, H. (2019a). Whole-rock geochemistry of the Vila Pouca de Aguiar granitic porphyries (northern Portugal), integrated with petrographic and SEM-EDS analysis. In *Livro de Resumos do XII Congresso Ibérico de Geoquímica e X Semana de Geoquímica, Évora, 22 a 25 de setembro de 2019*, pages 115–118, Estremoz, Portugal. Pólo de Estremoz da Universidade de Évora.

Oliveira, A., Martins, H. C. B., and Sant'Ovaia, H. (2020). Insights into the felsic vein magmatism in northern Portugal (Central Iberian Zone): an integrated geochemical and petrophysical study. In *20th International Multidisciplinary Scientific GeoConference, SGEM 2020, Conference Proceedings*, volume 20(1.1), pages 139–146, Albena, Bulgaria. STEF92 Technology. ISBN: 978-619-7603-04-0, ISSN: 1314-2704.

Oliveira, A., Sant'Ovaia, H., and Martins, H. C. B. (2019b). Anisotropia de Suscetibilidade Magnética do pórfiro granítico de Loivos (Vila Pouca de Aguiar, norte de Portugal). In *MagIber XI – Livro de Resumos, Condeixa-a Nova, 4 a 7 de setembro de 2019*, pages 102–105, Condeixa-a-Nova, Portugal. Universidade de Coimbra, Faculdade de Ciências e Tecnologia, Departamento de Ciências da Terra. ISBN: 978-989-98914-7-0.

Orejana, D., Villaseca, C., Billström, K., and Paterson, B. A. (2008). Petrogenesis of Permian alkaline lamprophyres and diabases from the Spanish Central System and their geodynamic context within western Europe. *Contrib. Mineral. Petrol.*, 156(4), 477–500.

Peppard, D. F., Mason, G. W., and Lewey, S. (1969). A tetrad effect in the liquid–liquid extraction ordering of lanthanides (III). *J. Inorg. Nucl. Chem.*, 31(7), 2271–2272.

Pin, C. and Santos Zalduegui, J. F. (1997). Sequential separation of light rare-earth elements, thorium and uranium by miniaturized extraction chromatography: application to isotopic analyses of silicate rocks. *Anal. Chim. Acta*, 339(1–2), 79–89.

Rämö, O. T. and Haapala, I. (1995). One hundred years of rapakivi granite. *Mineral. Petrol.*, 52(3–4), 129–185.

Ribeiro, M. L., Castro, A., Almeida, A., González Menéndez, L., Jesus, A., Lains, J. A., Lopes, J. C., Martins, H. C. B., Mata, J., Mateus, A., Moita, P., Neiva, A. M. R., Ribeiro, M. A., Santos, J. F., and Solá, A. R. (2019). Variscan magmatism. In Quesada, C. and Oliveira, J. T., editors, *The Geology of Iberia: A Geodynamic Approach, Volume 2: The Variscan Cycle*, Regional Geology Reviews, pages 497–526. Springer, Cham, Switzerland.

Sant'Ovaia, H., Bouchez, J. L., Noronha, F., Leblanc, D., and Vigneresse, J. L. (2000). Composite laccol-

ith emplacement of the post-tectonic Vila Pouca de Aguiar granite pluton (northern Portugal): a combined AMS and gravity study. *Earth Environ. Sci. Trans. R. Soc. Edinb.*, 91(1–2), 123–137.

Sant'Ovaia, H., Ribeiro, M. A., Martins, H., and Noronha, F. (2011). *Carta Geológica de Portugal na escala 1:50,000 e Notícia Explicativa da folha 6-D (Vila Pouca de Aguiar)*. Laboratório Nacional de Energia e Geologia, Lisbon, Portugal.

Sarjoughian, F., Kananian, A., Haschke, M., and Ahmadian, J. (2015). Transition from I-type to A-type magmatism in the Sanandaj-Sirjan Zone, NW Iran: an extensional intra-continental arc. *Geol. J.*, 51(3), 387–404.

Seltmann, R. and Müller, A. (2002). The Eastern Erzgebirge Granite Pluton: From Mantled Feldspars to Snowball Quartzes. *Mineral. Soc. Poland Spec. Pap.*, 20, 41–43.

Silva, A. and Ribeiro, M. L. (1991). *Notícia Explicativa da Folha 15-A (Vila Nova de Foz Côa) da Carta Geológica de Portugal na Escala 1: 50,000*. Serviços Geológicos de Portugal, Lisbon, Portugal.

Silva, A. F., Santos, A. J., Ribeiro, A., and Ribeiro, L. (1990). *Carta Geológica de Portugal na escala 1:50,000 – folha 15-A – Vila Nova de Foz Côa*. Serviços Geológicos de Portugal, Lisbon, Portugal.

Simons, B., Andersen, J. C., Shail, R. K., and Jenner, F. E. (2017). Fractionation of Li, Be, Ga, Nb, Ta, In, Sn, Sb, W and Bi in the peraluminous Early Permian Variscan granites of the Cornubian Batholith: Precursor processes to magmatic-hydrothermal mineralisation. *Lithos*, 278–281, 491–512.

Štemprok, M., Dolejš, D., Müller, A., and Seltmann, R. (2008). Textural evidence of magma decompression, devolatilization and disequilibrium quenching: an example from the Western Krušné hory/Erzgebirge granite pluton. *Contrib. Mineral. Petrol.*, 155(1), 93–109.

Stimac, J. and Hickmott, D. (1994). Trace-element partition coefficients for ilmenite, orthopyroxene and pyrrhotite in rhyolite determined by micro-PIXE analysis. *Chem. Geol.*, 117(1–4), 313–330.

Stimac, J. A. and Wark, D. A. (1992). Plagioclase mantles on sanidine in silicic lavas, Clear Lake, California: Implications for the origin of rapakivi texture. *Geol. Soc. Am. Bull.*, 104(6), 728–744.

Stull, R. J. (1979). Mantled feldspars and synneusis. *Am. Mineral.*, 64, 514–518.

Vaasjoki, M., Rämö, O. T., and Sakko, M. (1991). New U-Pb ages from the Wiborg rapakivi area: constraints on the temporal evolution of the rapakivi granite-anorthosite-diabase dyke association of southeastern Finland. *Precambrian Res.*, 51(1–4), 227–243.

Vernon, R. H. (2004). *A Practical Guide to Rock Microstructure*. Cambridge University Press, UK. ISBN: 052181443X.

Vernon, R. H. (2016). Rapakivi granite problems: plagioclase mantles and ovoid megacrysts. *Aust. J. Earth Sci.*, 63(6), 675–700.

Wang, S. J., Schertl, H. P., and Pang, Y. M. (2020). Geochemistry, geochronology and Sr–Nd–Hf isotopes of two types of early Cretaceous granite porphyry dykes in the Sulu orogenic belt, eastern China. *Can. J. Earth Sci.*, 57(2), 249–266.

Wark, D. A. and Stimac, J. A. (1992). Origin of mantle (rapakivi) feldspars: Experimental evidence of a dissolution- and diffusion-controlled mechanism. *Contrib. Mineral. Petrol.*, 111(3), 345–361.

Werner, M. and Cook, N. J. (2001). Nb-rich brookite from Gross Brukkaros, Namibia: substitution mechanisms and Fe^{2+}/Fe^{3+} ratios. *Mineral. Mag.*, 65(3), 437–440.

Whalen, J. B., Currie, K. L., and Chappell, B. W. (1987). A-type granites: geochemical characteristics, discrimination and petrogenesis. *Contrib. Mineral. Petrol.*, 95(4), 407–419.

Wu, F., Liu, X., Ji, W., Wang, J., and Yang, L. (2017). Highly fractionated granites: Recognition and research. *Sci. China Earth Sci.*, 60(7), 1201–1219.

Zhu, X. K. and O'Nions, R. K. (1999). Monazite chemical composition: some implications for monazite geochronology. *Contrib. Mineral. Petrol.*, 137(4), 351–363.